FKBP35 secures ribosome homeostasis in *Plasmodium falciparum*

Basil T. Thommen[1,2], Jerzy M. Dziekan[3], Fiona Achcar[4,5], Seth Tjia[3], Armin Passecker[1,2], Katarzyna Buczak[2], Christin Gumpp[1,2], Alexander Schmidt[2], Matthias Rottmann[1,2], Christof Grüring[1,2], Matthias Marti[4,5], Zbynek Bozdech[3], Nicolas M. B. Brancucci[1,2]

[1]Department of Medical Parasitology and Infection Biology, Swiss Tropical and Public Health Institute, 4123 Allschwil, Switzerland.

[2]University of Basel, 4001 Basel, Switzerland.

[3]School of Biological Sciences, Nanyang Technological University, Singapore.

[4]Wellcome Center for Integrative Parasitology, Institute of Infection, Immunity and Inflammation, University of Glasgow, Glasgow, UK.

[5]Institute for Parasitology, VetSuisse and Medical Faculty, University of Zurich, Zurich, Switzerland.

Correspondence:
Nicolas M. B. Brancucci, nicolas.brancucci@swisstph.ch

Keywords: malaria, *Plasmodium falciparum*, ribosome homeostasis, FKBP35, FK506, CETSA, antimalarial drugs

ABSTRACT

Plasmodium falciparum accounts for the majority of over 600'000 malaria-associated deaths annually. Parasites resistant to nearly all antimalarials have emerged and the need for drugs with alternative modes of action is thus undoubted. The FK506-binding protein *Pf*FKBP35 has gained attention as a promising drug target due to its high affinity to the macrolide compound FK506 (tacrolimus). Whilst there is considerable interest in targeting *Pf*FKBP35 with small molecules, a genetic validation of this factor as a drug target is missing and its function in parasite biology remains elusive. Here, we show that limiting *Pf*FKBP35 levels are lethal to *P. falciparum* and result in a delayed-death phenotype that is characterized by defective ribosome homeostasis and stalled protein translation. We furthermore show that FK506, unlike the role of this drug in model organisms, exerts its anti-proliferative activity in a *Pf*FKBP35-independent manner and, using cellular thermal shift assays, we identify FK506-targets beyond *Pf*FKBP35. In addition to revealing first insights into the function of *Pf*FKBP35, our results show that FKBP-binding drugs can adopt non-canonical modes of action – with major implications for the development of FK506-derived molecules active against *Plasmodium* parasites and other eukaryotic pathogens.

37 # 1 Introduction

38 Despite considerable progress in recent years, malaria remains one of the major global health
39 threats (1). The apicomplexan parasite *Plasmodium falciparum* is responsible for the vast
40 majority of the over 600'000 malaria deaths in 2020. Most of this burden is carried by infants
41 and children under the age of five in sub-Saharan Africa. Malaria deaths increased by 12%
42 compared to 2019, which can at least in part be explained by the COVID-19 related suspension
43 of malaria control and treatment measures (1). In addition, the emergence of parasites resistant
44 to most antimalarials, including artemisinin-based combination therapies, endangers current
45 and future disease elimination efforts and underscores the need for developing drugs with
46 alternative modes of action (2).

47 FK506 (tacrolimus), a well-characterized immunosuppressant, shows considerable activity
48 against asexual blood stage parasites (3). *P. falciparum* encodes a single FK506-binding protein
49 (FKBP) dubbed *Pf*FKBP35 (PF3D7_1247400), which is considered to be a promising drug
50 target (4, 5). FKBPs belong to the immunophilin family and are conserved throughout the
51 eukaryotic kingdom (6, 7). In contrast to the malaria parasite, most other eukaryotes encode
52 several FKBPs that, besides showing high affinity for the FK506 drug, exert peptidyl-prolyl
53 isomerase (PPIase) activity. The PPIase moiety catalyzes cis-trans isomerization of proline
54 residues – an event thought to be rate-limiting for the folding of many proteins (8). Independent
55 of their PPIase activity, FKBPs act as chaperones to prevent protein aggregation under stress
56 conditions (9, 10). Furthermore, some FKBP variants play a role in cellular signaling or gene
57 regulation (11, 12). Human FKBP12 for instance is best-known for its ability to form a complex
58 with the immunosuppressant drugs FK506 and rapamycin. These complexes inhibit the
59 phosphatase activity of calcineurin and the kinase activity of mTOR (mechanistic target of
60 rapamycin), respectively (13). Amongst many other effects, this inhibition results in decreased
61 T-cell activation. Of note, the regulatory role of *Hs*FKBP12 depends on the presence of
62 rapamycin or FK506. In absence of drugs, this immunophilin neither interacts with mTOR nor
63 with calcineurin and does hence not affect activity of these key components of eukaryotic cells.
64 Due to the conserved nature of FKBPs, rapamycin and FK506 have also gained attention as
65 potential antimicrobial drugs (3, 7).

66 Similar to its homologs in model organisms, *Pf*FKBP35 harbors PPIase and chaperoning
67 activity *in vitro* (5). Despite sharing key features with FKBPs of other eukaryotes, its role in *P.*
68 *falciparum* remains elusive. *Pf*FKBP35 is believed to interact with heat shock proteins (HSPs)
69 and co-immunoprecipitates with cytoskeletal factors of *P. falciparum* (14). While *Pf*FKBP35

70 is inhibiting the phosphatase activity of recombinant calcineurin in a FK506-independent
71 manner (15-17), it does not co-localize with calcineurin *in vivo* (16). The protein is expressed
72 throughout the 48-hour intra-erythrocytic development of *P. falciparum* and is found within the
73 cytosol of ring stage parasites. In the older trophozoite and the replicating schizont stages, the
74 protein was reported to also localize to the nucleus (16). While a transposon-based mutagenesis
75 screen suggests that *Pf*FKBP35 is essential for intra-erythrocytic replication (18), neither its
76 cellular function nor its essentiality was confirmed experimentally in live parasites. The
77 unknown role in parasite biology notwithstanding, *Pf*FKBP35 is considered to be a viable drug
78 target and, given the fact that *P. vivax* and *P. knowlesi* encode FKBP homologs that exhibit
79 comparable PPIase activities (19, 20), future FKBP-targeted therapies may be effective across
80 different *Plasmodium* species.

81 Crystal structures of *Pf*FKBP35 in complex with FK506 and rapamycin revealed high affinity
82 interactions with the FK506-binding domain of the protein (15, 21, 22). Consistent with these
83 observations, *in vitro* enzyme activity assays showed that FK506 inhibits the PPIase activity of
84 recombinant *Pf*FKBP35 in a dose-dependent manner (5). Previous research aimed at exploiting
85 structural differences between human and parasite-encoded FKBPs to circumvent the
86 immunosuppressive activity of drug-bound *Hs*FKBP12 (23-26). These efforts include
87 investigation of non-covalent FKBP inhibitors such as adamantyl derivatives, macrocycles, the
88 small molecule D44 (23-25, 27, 28) and the synthetic ligand for FKBP (SLF) as well as
89 derivatives thereof designed to covalently bind *Pf*FKBP35 (29). While D44 shows promising
90 antimalarial activity, it fails to alter thermostability of the FK506-binding domains of
91 *Pf*FKBP35 and *Hs*FKBP12 *in vitro* (29), suggesting that this compound does not directly
92 interact with *Pf*FKBP35. Up until now, *Pf*FKBP35 has not been validated as a drug target using
93 reverse genetics, and the link between *Pf*FKBP35-interacting drugs and their antimalarial
94 activity remains elusive (3).

95 Here, we generated inducible *Pf*FKBP35 knock-out, knock-down as well as over-expression
96 cell lines and show that *Pf*FKBP35 is essential for asexual replication of blood forms. We
97 demonstrate that *Pf*FKBP35 is vital for ribosome homeostasis on the post-transcriptional level
98 and likely acts as a chaperone during the biogenesis of ribosomes in the nucleus. As a result,
99 *Pf*FKBP35 knock-out parasites stall protein translation prior to dying at the early schizont stage,
100 which underpins the potential of *Pf*FKBP35 as a drug target. Using cellular thermal shift assays
101 (CETSA), we corroborate the high affinity binding of FK506 to *Pf*FKBP35 and reveal
102 interactions of the *Pf*FKBP35/FK506 pair with ribosome-associated proteins. Importantly,

103 however, our data demonstrate that FK506 fails at inhibiting the essential function of
104 *Pf*FKBP35 and exerts its antimalarial activity in a *Pf*FKBP35-independent manner. While this
105 has major implications for the development of future FK506-based antimalarials and/or
106 *Pf*FKBP35-inhibiting drugs, we identify putative targets of FK506 beyond *Pf*FKBP35 in *P.*
107 *falciparum*.

108

109 # 2 Results

110 ## 2.1 *Pf*FKBP35 is essential for asexual replication

111 In a first step, using CRISPR/Cas9-mediated gene editing, we engineered a *P. falciparum* cell
112 line allowing for a conditional knock-down of *Pf*FKBP35 using the DD/Shield system (30, 31)
113 (Figs. 1A and S1A-B). Despite the efficient depletion of *Pf*FKBP35 under knock-down
114 conditions, parasites did not show apparent growth defects (Figs. S1C-D). Immunofluorescence
115 assays (IFA) showed that *Pf*FKBP35 localizes to distinct foci within the parasite nucleus (Fig.
116 1B).

117 Next, we generated a cell line allowing for the conditional knock-out of the endogenous coding
118 sequence using a dimerizable Cre recombinase (DiCre)-based system (32). Specifically, we
119 introduced two *loxP* sites – one within a synthetic intron (33) downstream of the start codon
120 and one after the stop codon of the *fkbp35* coding region – and added a *green fluorescent protein*
121 (*gfp*) sequence downstream of this expression cassette (Figs. 1C, S2A). As a result, these
122 NF54/iKO-FKBP35 parasites express tag-free, wild-type (WT) *Pf*FKBP35 protein under
123 control conditions (FKBP35^{WT}). Upon DiCre activation, the *loxP* sites are recombined and the
124 *fkbp35* locus is excised from the parasite genome (Figs. 1C, S2B). Under these knock-out
125 conditions (FKBP35^{KO}), parasites express cytosolic GFP under control of the endogenous
126 *fkbp35* promoter. This setup allows monitoring knock-out efficiency at the single cell level and
127 revealed that DiCre successfully deleted *fkbp35* in the vast majority of parasites (Fig. 1D).

128 In a first attempt, we induced the *fkbp35* knock-out in synchronous ring stage NF54/iKO-
129 FKBP35 parasites at 0-6 hours post erythrocyte invasion (hpi), i.e. prior to the expected peak
130 transcription of *fkbp35* (34). These FKBP35^{KO} parasites showed a delayed death phenotype:
131 parasites completed intra-erythrocytic development in the first generation (G1) without
132 noticeable effects (Fig. 1E) and entered the next generation (G2) with a multiplication rate
133 similar to that of the FKBP35^{WT} control population (Fig. 1F). In G2, however, FKBP35^{KO}
134 parasites arrested at the late trophozoite/early schizont stage (approximately 30-36 hpi) with

135 many cells failing to enter DNA replication in the S-phase (Fig. 1E). To investigate this
136 phenomenon in more detail, we induced the *fkbp35* knock-out at three different time points
137 during the IDC. Similar to DiCre activation at 0-6 hpi, knocking out *fkbp35* at 12-18 hpi resulted
138 in parasite death at the trophozoite/schizont stage of the subsequent generation. However, when
139 induced at 24-30 hpi or 34-40 hpi in G1, parasites did not only complete the current IDC but
140 also successfully passed through G2 before they eventually arrested in G3 (Fig. 1G).
141 Considering that low *Pf*FKBP35 levels are sufficient to maintain the essential function of the
142 protein, as observed with the NF54/iKD-FKBP35 parasites (see Fig. S1C-D), it is conceivable
143 that proteins expressed between 0 and 24hpi, i.e. prior to deleting *fkbp35* from the genome,
144 allow parasites to enter G3.

145 The delayed death of FKBP35^{KO} is reminiscent of a phenotype observed in apicoplast-deficient
146 parasites (35, 36). We therefore tested if *Pf*FKBP35 is involved in apicoplast biology, but did
147 not find evidence for an association with this organelle (Fig. S2C). Furthermore, given the
148 reported interaction of *Pf*FKBP35 with heat shock proteins (14, 16), we also tested the parasite`s
149 response to heat stress, but could not detect altered heat-susceptibility between FKBP35^{KO} and
150 FKBP35^{WT} cells (Fig. S2D).

151

152 **2.2 *Pf*FKBP35 is crucial for ribosome homeostasis and protein translation**

153 To further elucidate the function of *Pf*FKBP35, we induced the *fkbp35* knock-out in early ring
154 stages (0-6 hpi) and compared the proteomes of FKBP35^{KO} and FKBP35^{WT} parasites at the
155 schizont stage of G1 (36-42 hpi) and at the trophozoite stage of the following generation (G2,
156 24-30 hpi) using a quantitative proteomics approach.

157

158 **2.2.1 The knock-out of *Pf*FKBP35 causes accumulation of pre-ribosome components in G1**

159 Consistent with the efficient deletion of *fkbp35* on the genomic level, FKBP35^{KO} schizonts of
160 G1 showed a 19-fold (18.9 +/-5.7 s.d.) reduction of FKBP35 and GFP levels were increased by
161 84-fold (83.7 +/-38.5 s.d.) when compared to the control population (Fig. 2A, Table S1).
162 Besides *Pf*FKBP35 and GFP, 50 parasite proteins were significantly deregulated in FKBP35^{KO}
163 schizonts and 34 of them found at elevated levels compared to the FKBP35^{WT} control
164 conditions. A gene ontology analysis using PANTHER (37) indicated enrichment of the "*pre-*
165 *ribosome*" (fold enrichment = 30.4, p-value = 1.46E-5, 4/34 proteins) and "*nucleolus*" (fold
166 enrichment = 6.77, p-value = 8.85E-4, 5/34 proteins) terms among these factors. While the pre-

167 ribosome is a large subunit precursor of mature ribosomes, the nucleolus represents the primary
168 site for the biogenesis of ribosomal subunits (38). In contrast to factors being more abundant in
169 knock-out parasites, none of the 16 factors with lower abundance in FKBP35^{KO} cells were
170 associated with ribosome-related processes (Table S1). Despite being phenotypically silent in
171 G1, the accumulation of pre-ribosome and nucleolar components hints at perturbed ribosome
172 maturation in these cells. Specifically, it is conceivable that the observed buildup of ribosome
173 intermediates results from reduced anabolic activity, i.e. the stalling of nucleolar pre-ribosome
174 assembly.

175 Notwithstanding these effects, FKBP35^{KO} cells were equally sensitive to the translation
176 inhibitor cycloheximide compared to their FKBP35^{WT} counterparts (Fig. 2B), indicating that
177 ribosome function is not compromised at this point in time (39). This is consistent with normal
178 cell cycle progression in G1 and unaltered multiplication rates of FKBP35^{KO} parasites, as
179 described above (see Figs. 1E-F), and shows that the prominent depletion of *Pf*FKBP35 does
180 not have a major impact on parasite viability in G1.

181

182 **2.2.2 *Pf*FKBP35 is essential for maintaining normal levels of functional ribosomes in G2**

183 In the following generation (G2, 24-30 hpi), the proteome of FKBP35^{KO} trophozoites showed
184 substantial differences. Despite the absence of morphological changes at this point in time, 216
185 proteins were significantly deregulated (Fig. 2C). Among these, 50 proteins were found at
186 higher abundance compared to FKBP35^{WT} and their gene ontology terms point towards an
187 effect on processes involved in energy metabolism (Fig. 2D).

188 The majority of deregulated factors (166 of 216) in G2, however, were less abundant in
189 FKBP35^{KO} compared to the FKBP35^{WT} control cells. Very prominently, 20 of the top 50 hit
190 molecules are ribosomal proteins that, on average, show a two-fold reduction (2.0 +/- 0.4 s.d.)
191 in FKBP35^{KO} parasites (Table S1). It is therefore not surprising that PANTHER identified the
192 knock-out of *Pf*FKBP35 to mainly affect ribosome-related processes, such as "*cytoplasmic*
193 *translation*", "*ribosome assembly*", and "*ribosomal large subunit biogenesis*" (Fig. 2D) (37).

194 To assess if the reduced levels of ribosomal proteins result in lower protein translation rates,
195 we employed the "surface sensing of translation" (SUnSET) technique. SUnSET is based on
196 incorporation of the tyrosyl-tRNA analogue puromycin into nascent peptide chains and thereby
197 allows monitoring newly synthesized proteins (40). As expected, we found that FKBP35^{KO}
198 trophozoites in G2 (24-30 hpi) showed reduced translation rates compared to the FKBP35^{WT}

199 control population (Fig. 2E). Further, protein synthesis was not affected in parasites of the
200 parental line NF54/DiCre following DiCre activation using rapamycin (S2E), demonstrating
201 that translation is impaired in response to knocking out *Pf*FKBP35.

202 Taken together, these results indicate that, under knock-out conditions, *Pf*FKBP35 levels
203 become limiting for ribosome maturation late during schizogony of G1, without having
204 immediate effects on the steady-state levels of mature ribosomes. The knock-out of *Pf*FKBP35
205 is thus phenotypically silent in G1. In absence of a continuous supply of mature ribosomes
206 under FKBP35^{KO} conditions, however, FKBP35^{KO} parasites fail at synthesizing protein at
207 levels that would support normal parasite development in the next generation (G2).

208

209 **2.3 The knock-out of *Pf*FKBP35 is transcriptionally silent**

210 To examine if the altered proteome of FKBP35^{KO} parasites is the result of *Pf*FKBP35-
211 controlled transcription, we compared the transcriptional profiles of FKBP35^{WT} and
212 FKBP35^{KO} in a time course RNA-Sequencing (RNA-Seq) experiment spanning two IDCs.
213 Specifically, we induced the knock-out of FKBP35 in synchronous parasites at 0-6 hpi and
214 collected RNA from parasite populations at three and four subsequent time points (TPs) in G1
215 and G2, respectively (Figs. 3A, S3A). With the exception of TP7, these time points cover a time
216 frame during which FKBP35^{KO} cells cannot be distinguished from their FKBP35-expressing
217 counterparts on a morphological level (compare Fig. 1E).

218 As expected, the transcriptome of FKBP35^{KO} showed a prominent reduction of steady-state
219 *fkbp35* transcripts already in TP1 (11.3-fold +/-2.0 s.d.) compared to the FKBP35^{WT} control
220 population (Fig. S3B, Table S2). During peak transcription at 30-36 hpi (TP2), this difference
221 increased to 240-fold (238.4 +/-20.0 s.d.) and, consistent with the efficient recombination at the
222 *fkbp35* locus, these cells started transcribing *gfp*. Notwithstanding the prominent depletion of
223 *fkbp35* transcripts, the transcriptome of FKBP35^{KO} is only marginally affected up to and
224 including 24-30 hpi in G2 (TP6). By contrast, at 30-36 hpi (TP7) the transcription of knock-out
225 parasites shows major changes (Fig. 3B). Considering the appearance of morphological changes
226 in FKBP35^{KO} at this time point, effects on the transcriptome are unlikely to represent specific
227 activities of *Pf*FKBP35 in gene regulation. Indeed, mapping the transcriptome of individual
228 time points to a high resolution reference (41), revealed a significant slow-down of FKBP35^{KO}
229 compared to FKBP35^{WT} parasites at TP7 (Figs. 3C, S3C). This indicates aborted cell cycle
230 progression in FKBP35^{KO} parasites during a phase that is characterized by a rapid increase in

231 biomass – possibly due to a translation and/or size-dependent cell cycle checkpoint (42). At
232 earlier time points (TP1-TP6), the transcriptomes of FKBP35^{KO} and FKBP35^{WT} are
233 comparable and the differences observed on the level of individual genes clearly fail at
234 explaining the proteomic changes observed in FKBP35^{KO} parasites at 24-30 hpi in G2 (TP6),
235 reiterating that the essential activity of *Pf*FKBP35 is linked to post-transcriptional processes.

236

237 **2.4 FKBP-targeting drugs fail at inhibiting the essential function of *Pf*FKBP35**

238 *Pf*FKBP35 emerged as a promising antimalarial drug target (4) and considerable efforts were
239 made to define interactions of this immunophilin with small molecules in the last decade (24-
240 26, 43). Several studies conclusively demonstrated that FK506 – the most well-known ligand
241 of mammalian FKBPs (44) – binds to *Pf*FKBP35 (15, 21, 22) and kills asexual blood stage
242 parasites with a half-maximal inhibitory concentration (IC50) in the low micromolar range at
243 1.9 µM (3).

244 Considering the proposed direct interaction between FK506 and FKBP35 in *P. falciparum*, we
245 expected that FKBP35^{KO} parasites show altered sensitivity to the drug. Consistent with
246 published data, FK506 killed FKBP35^{WT} cells with an IC50 of 1942 nM (+/-193 nM s.d.) when
247 administered at 0-6 hpi (Fig. 4A). Surprisingly however, and despite the prominent depletion
248 of the protein under knock-out conditions, FKBP35^{KO} and FKBP35^{WT} parasites were equally
249 sensitive to FK506 (IC50 = 1741 +/- 187) (Fig. 4A). Similarly, neither the efficient knock-down
250 of *Pf*FKBP35 in NF54/iKD-FKBP35 parasites (compare Fig. S1C), nor its over-expression
251 (OE) in NF54/iOE-FKBP35 cells (Fig. S4A-C), resulted in the expected sensitivity change to
252 FK506 treatment (Fig. 4B). In addition to this apparent independence of the drug to varying
253 *Pf*FKBP35 levels, and in agreement with earlier studies (3, 24, 45), FK506 unfolds its
254 antimalarial activity fairly quickly, i.e. within the same cycle after treatment. Standing in stark
255 contrast to the delayed death phenotype of FKBP35^{KO} parasites (compare Fig. 1E-G), this
256 immediate activity on parasite survival substantiates the notion that FK506 must target essential
257 parasite factors other than *Pf*FKBP35.

258 To rule out that the timing of drug exposure is masking expected links between FK506 and
259 *Pf*FKBP35, we tested whether administering FK506 at 30-36 hpi (instead of 0-6 hpi) affects
260 parasite survival in a *Pf*FKBP35-dependent manner. However, we did not observe a change
261 compared to FKBP35^{WT} parasites (Fig. S5A), ruling out the possibility that FKBP35^{KO}
262 parasites were killed by FK506 before *Pf*FKBP35 levels were different in the two populations.

263 Further, to account for a scenario in which the activity of FK506 on *Pf*FKBP35 is masked by a
264 temporal delay between drug exposure and parasite killing, we induced the knock-out of
265 *Pf*FKBP35 at 34-40 hpi (instead of 0-6 hpi) and allowed FKBP35^{KO} parasites to proceed to G2,
266 before exposing them to different FK506 concentrations. Despite these efforts, FKBP35^{WT} and
267 FKBP35^{KO} parasites were equally sensitive to FK506 (Fig. S5B, S5C) and the calcineurin
268 inhibitor cyclosporin A (Fig. S5D-E).

269 In addition to FK506, we evaluated the *Pf*FKBP35-specific inhibitor D44 (N-(2-Ethylphenyl)-
270 2-(3h-Imidazo[4,5-B]pyridin-2-Ylsulfanyl)acetamide) but, surprisingly, we failed to reproduce
271 the previously reported dose-response effect (24). We tested D44 from two suppliers using
272 NF54/iKO-FKBP35, NF54 wild type and K1 parasite strains using different assay setups,
273 including the gold standard method that is based on the incorporation of tritium labeled
274 hypoxanthine into DNA of replicating cells (46). Still, we could not detect any activity of D44
275 on asexual replication of blood stage parasites (Figs. S5F-G).

276 Taken together, these results are in clear conflict with the perception that FK506 and D44 target
277 the essential activity of *Pf*FKBP35.

278

279 **2.5 Probing FK506 interactions in Cellular Thermal Shift Assays (CETSA)**

280 Considering the unaltered activity of FK506 in FKBP35^{KO} compared to FKBP35^{WT} parasites,
281 we reasoned that FK506 must target proteins other than *Pf*FKBP35. To identify potential targets
282 of the drug in *P. falciparum*, we used the *cellular thermal shift assay followed by mass*
283 *spectrometry* (MS-CETSA). This approach exploits the fact that, once drug-protein complexes
284 are formed, thermostability of the target protein is altered (47). We applied the so-called
285 *isothermal dose-response* variant of CETSA using FK506 (48). Here, target proteins are
286 identified based on their dose-dependent stabilization by drugs under thermal challenge
287 (different temperatures) when compared to a non-denaturing condition (37 °C), using the
288 change in the area under the curve (ΔAUC) and the dose-response curve goodness of fit (R^2) as
289 metrics (Fig. 4C) (48).

290 **2.5.1 CETSA identifies targets of FK506**

291 In a first step, we performed CETSA in combination with drug-exposed protein extracts. Since
292 proteins lose their physiological context during the process of protein extraction, this variant of
293 the CETSA approach is designed to identify direct protein-drug interactions (47, 48). Not

294 surprisingly, we found *Pf*FKBP35 to be stabilized by FK506 in a dose-dependent manner when
295 challenged at 60 °C with an EC50 of 152.0 nM (Fig. 4D). The fact that FK506 exhibits its
296 stabilizing activity already in the low nanomolar concentration range indicates high affinity
297 interactions between the protein-drug pair. This FK506-mediated stabilization of *Pf*FKBP35 is
298 thus achieved at drug concentrations that are magnitudes below the IC50 of FK506 in parasite
299 survival assays (1942 nM +/-193 nM s.d.) (compare Fig. 4A). In line with several previous
300 reports on the *Pf*FKBP35/FK506 pair *in vitro*, our results show that, indeed, FK506 is binding
301 to *Pf*FKBP35, but in contrast to previous assumptions this interaction fails at explaining the
302 antimalarial activity of FK506.

303 Besides *Pf*FKBP35, FK506 stabilizes a number of other proteins in a dose-dependent manner
304 (Figs. 4E and S6). A few of these factors show pronounced sigmoidal stabilization profiles and
305 are predicted to be essential (Fig. 4E) (18). Amongst others, N6-methyl transferase MT-A70
306 (PF3D7_0729500), histone deacetylase HDA2 (PF3D7_1008000), pre-mRNA-splicing factor
307 CEF1 (PF3D7_1033600), FeS cluster assembly protein SufD (PF3D7_1103400) and the
308 H/ACA ribonucleoprotein complex subunit 1 (PF3D7_1309500) showed most pronounced
309 stabilization profiles (Fig. S6 and Table S3). In contrast to *Pf*FKBP35, most of these likely
310 essential candidates are stabilized at FK506 concentrations close to the drug`s IC50 (compare
311 Fig. 4A). It is therefore tempting to speculate that the binding of FK506 to at least one of these
312 factors is responsible for the antimalarial activity of the drug.

313 **2.5.2 The *Pf*FKBP35/FK506 pair interferes with ribosomal complexes**

314 Given the high-affinity interaction of *Pf*FKBP35 with FK506 and its association with ribosomal
315 proteins, we set out to describe the native context of *Pf*FKBP35 using the live cell variant of
316 CETSA. In contrast to focusing exclusively on direct protein-drug interactions, live cell CETSA
317 allows capturing drug-induced shifts in protein stability beyond those of direct binding partners
318 (48) and amongst others allows identifying factors present in the same protein complex as the
319 target protein. To do so, CETSA takes advantage of the fact that factors within complexes have
320 similar denaturation temperatures due to their co-aggregation upon heat-induced denaturation
321 (49). As a consequence, this CETSA variant generally identifies more factors compared to the
322 protein extract-based CETSA approach (Fig. 4C).

323 As expected, and confirming the results above, live cell CETSA shows that FK506 alters the
324 thermal stability of *Pf*FKBP35 already at very low drug concentrations when challenged at 60
325 °C with an EC50 of 286.7 nM (Fig. 4D). Interestingly, and in contrast to the protein lysate-

326 based approach, live cell CETSA revealed that more than 50 ribosomal proteins are stabilized
327 in presence of FK506 when challenged at 55°C, with a median EC50 of 45.9 nM (25th percentile
328 = 34.2, 75th percentile = 58.9). Of note, these ribosomal proteins were stabilized at virtually
329 identical FK506 concentrations (Figs. 4F, and S7), indicating that the drug – directly or
330 indirectly – interacts with ribosomal complexes. This is in further agreement with the fact that
331 these ribosomal factors were not identified by protein lysate-based CETSA (compare Figs. 4C,
332 S6).

333 Worth mentioning, we observed a drug dose-dependent increase in soluble protein abundance
334 of ribosomal factors also under non-denaturing conditions, i.e. at 37 °C, with a median EC50
335 of 1.94 µM (25th percentile = 1.85, 75th percentile = 2.1) (Figs. 4F, S7). Generally, due to the
336 absence of a denaturing heat challenge, such a drug-dependent enrichment in soluble protein
337 levels does not indicate binding-induced thermal stabilization of proteins (48). Instead, this can
338 be the result of increased protein synthesis, altered protein conformation or, alternatively, occur
339 in response to factors disengaging from larger protein complexes. The fact that FK506
340 solubilizes a high number of ribosomal proteins within a very narrow concentration window
341 also at 37 °C, implies that these factors are liberated from the same ribosomal complex or from
342 complexes that interact with each other and shows that FK506 negatively affects stability of
343 ribosomal structures in live cells. However, these effects are limited to high, presumably
344 saturating FK506 concentrations, likely explaining why the drug fails at killing parasites in a
345 *Pf*FKBP35-dependent manner. Importantly, the vast majority of ribosomal proteins identified
346 in live cell CETSA are shared with those de-regulated in *Pf*FKBP35 knock out cells (Fig. 4G),
347 providing conclusive evidence for a shared localization of FK506 and its *Pf*FKBP35 target in
348 live parasites.

349 Together with the above-described importance of *Pf*FKBP35 in ribosome homeostasis, these
350 results strongly suggest that FK506 is recruited to the activity site of *Pf*FKBP35 – most
351 probably the nucleolar maturation sites of ribosomes – where it leads to a destabilization of
352 ribosomal complexes.

353

354 # 3 Discussion

355 Members of the FKBP family are involved in regulating diverse cellular processes in eukaryotic
356 as well as in prokaryotic cells (8, 50). In contrast to most other eukaryotes, the human malaria
357 parasite *P. falciparum* encodes a single FKBP only (16). The enzymatic activity of *Pf*FKBP35,

358 as well as the interactions of the protein with FKBP-targeting drugs, was subject to considerable
359 drug-focused research *in vitro*. Besides demonstrating the drug`s affinity to *Pf*FKBP35 by co-
360 crystallization, these efforts uncovered that FK506 inhibits enzymatic activity of the protein`s
361 PPIase domain (5). Together with the anti-malarial activity of FK506, these data offered
362 compelling evidence for an essential but yet uncharacterized role of *Pf*FKBP35 during blood
363 stage development of *P. falciparum*.

364 Here, we set out to investigate the role of *Pf*FKBP35 in parasite biology. Using an inducible
365 knock-out approach, we show that *Pf*FKBP35 is indeed essential for intra-erythrocytic
366 development of asexually replicating *P. falciparum* parasites and FKBP35^{KO} cells die during
367 the late trophozoite/early schizont stage. Surprisingly, these parasites display a delayed-death
368 phenotype that is independent of apicoplast function and only manifests in the cycle following
369 knock-out induction without affecting cell cycle progression in the first generation (G1) or
370 multiplication rates from G1 to G2. This contradicts the known effects of FK506 and other
371 *Pf*FKBP35-targeting drugs for two main reasons. First, these drugs exert their parasiticidal
372 activity within the same IDC (24). Second, neither the conditional knock-out, knock-down nor
373 the overexpression of *Pf*FKBP35 altered the parasite's sensitivity to FK506, even though levels
374 of the *Pf*FKBP35 target are profoundly deregulated in the respective mutant lines. Together,
375 these data show that the parasite-killing activity of FK506 is independent of the essential
376 function of *Pf*FKBP35. We hence aimed at the identification of other FK506 targets using
377 CETSA, as discussed further down.

378 Knocking out *Pf*FKBP35 early during intra-erythrocytic development has no effect on parasite
379 morphology in G1 and provokes only moderate changes on the protein level compared to
380 FKBP35^{WT} parasites. While the effects in G1 are relatively subtle, it is noticeable that
381 nucleolus-associated factors are found at higher abundance in knock-out cells. In the next cycle,
382 FKBP35^{KO} parasites show a dramatic decrease of factors associated with ribosome- and
383 translation-related processes during trophozoite development (G2, 24-30 hpi). Consistently,
384 protein translation in FKBP35^{KO} parasites is reduced considerably. Importantly, at this point in
385 time, FKBP35^{KO} cells still show ordinary morphology and their transcriptional activity remains
386 largely unaffected. The observed changes in the abundance of ribosomal factors must therefore
387 result from post-transcriptional activity of *Pf*FKBP35. While ribosomal components are present
388 at higher levels in G1, they are drastically reduced in FKBP35^{KO} cells in G2. These opposing
389 effects are peculiar, but likely result from *Pf*FKBP35 activity in a shared cellular process.
390 Specifically, it is conceivable that low *Pf*FKBP35 levels inhibit ribosome maturation in G1,

391 explaining the accumulation of (pre-) ribosomal factors. While the levels of functional
392 ribosomes are sufficient to support continued translation in G1, ribosomes likely become
393 limiting in the next generation (G2), which eventually results in stalled translation activity and
394 concomitant parasite death at the onset of schizogony; i.e. at a time when protein synthesis is
395 required for facilitating the steep increase in biomass.

396 In contrast to the significant effects on the protein level, the transcription of FKBP35^{KO} remains
397 largely unaffected by the loss of *Pf*FKBP35 and becomes apparent only during late
398 trophozoite/early schizont development in G2 (30-36 hpi); i.e. at a time during which cell cycle
399 progression is slowed down in FKBP35^{KO} parasites. In fact, at this stage the transcriptional
400 signature of FKBP35^{KO} parasites is dominated by the slowed progression through intra-
401 erythrocytic development, rather than resulting from specific gene regulatory events. While this
402 stalling is consistent with the observed effects on ribosome homeostasis and protein translation,
403 it demonstrates that, in contrast to certain FKBP family members in other organisms,
404 *Pf*FKBP35 does not have apparent roles in transcriptional control.

405 As discussed above, binding of FK506 to *Pf*FKBP35 cannot explain the drug's antimalarial
406 activity and our attempts to identify targets of FK506 using resistance selection failed. This
407 indicates that parasites do not readily acquire resistance mutations, possibly due to drug action
408 on multiple targets (51). We hence aimed at identifying other FK506 targets using CETSA. In
409 line with previous work on the drug *in vitro*, CETSA on *P. falciparum* protein extracts
410 confirmed that FK506 is targeting *Pf*FKBP35 with exceptionally high affinity in the low
411 nanomolar range. Considering this well-characterized FK506-*Pf*FKBP35 interaction (22) and
412 the resulting inhibition of its PPIase activity (5), unaltered drug sensitivity of *Pf*FKBP35
413 mutants indicates that PPIase activity is dispensable for blood stage parasites. Noteworthy,
414 PPIase-independent functions of FKBPs have been described in other systems. For instance,
415 PPIase activity of the *Escherichia coli* trigger factor (TF), a ribosome-associated FKBP, is not
416 required for protein folding (52). Similarly, human FKBP52 maintains its function as a
417 chaperone under PPIase-inhibiting conditions (9). While it is conceivable that PPIase activity
418 is dispensable for intra-erythrocytic development of *P. falciparum*, the enzymatic activity of
419 *Pf*FKBP35 may be compensated by other factors, e.g. by PPIase domain-harboring members
420 of the cyclophilin family (53).

421 CETSA performed on protein lysates identified a number of parasite factors binding to FK506.
422 Compared to the *Pf*FKBP35/FK506 pair, however, these interactions are of considerably lower
423 affinity. The adenosine-methyltransferase MT-A70 (PF3D7_0729500) and the pre-mRNA-

splicing factor CEF1 (PF3D7_1033600), for instance, were stabilized by FK506 with EC50 concentrations of 2.0 and 3.1 µM, respectively. While this affinity is relatively poor compared to the strong interaction formed between *Pf*FKBP35 and FK506, one should be cautious designating the binding of FK506 to these proteins as irrelevant "*off target*" effects. In fact, their inhibition may well be masked by high-affinity binding of FK506 to *Pf*FKBP35 – a possibility that shall briefly be discussed in the following section.

Assuming that FK506 is inhibiting the essential function of *Pf*FKBP35, one would expect parasites to show a delayed-death phenotype similar to that observed in FKBP35$^{\mathbf{KO}}$ parasites. In contrast to this delayed killing, the effect of FK506 on other essential targets likely manifests in the same cycle and would hence mask the effect of *Pf*FKBP35-inhibition. Consistent with this possibility, FK506 kills *P. falciparum* parasites at 1.9 µM (+/-0.2 µM s.d.), i.e. at concentrations similar to those required for stabilizing MT-A70 and CEF1 under thermal challenge in CETSA. Our attempts to prove that FK506 indeed inhibits essential functions of *Pf*FKBP35 failed: Neither knocking out *Pf*FKBP35 at different time points nor adding FK506 to different stages of FKBP35$^{\mathbf{KO}}$ parasites could provide evidence for a scenario in which *Pf*FKBP35-dependent effects are simply masked by "*off target*" effects (compare Fig. S5). This indicates that either the binding of FK506 does not interfere with the essential role of *Pf*FKBP35, or that *Pf*FKBP35 is inhibited only at high FK506 concentrations that also inhibit other essential factors. In this context it is worth mentioning that parasites remain unaffected by a highly efficient knock-down of endogenous *Pf*FKBP35 (observed with NF54/iKD-FKBP35; compare Figs. S1C-D), which demonstrates that very low protein levels are sufficient to maintain the essential function of *Pf*FKBP35. It is thus conceivable that high FK506 concentrations are required to fully inhibit *Pf*FKBP35 – a view that is further supported by data obtained with the live cell CETSA approach.

Besides identifying direct binding of drugs to their target, live cell CETSA allows capturing indirect effects on factors that act in the same pathway or in the same protein complex as the drug-bound target (48). While this approach confirmed the high affinity binding of FK506 to *Pf*FKBP35, it also revealed that more than 50 ribosomal proteins share a very prominent CETSA signature: First, they are thermally stabilized by FK506 within a narrow concentration window of the drug. Second, higher levels of FK506 increase the solubility of these ribosomal components also at 37 °C. These results indicate that the FK506/*Pf*FKBP35 pair interacts with ribosomal complexes and that FK506 is able to induce the dissociation of these ribosomal structures under physiological conditions. Importantly, and in contrast to the binding of FK506

457 to *Pf*FKBP35, this effect on ribosomes is only observed at high concentrations of the drug.
458 Together, these data likely explain the discrepancy observed between the high binding affinity
459 of FK506 for *Pf*FKBP35 and the low or even absent effect of the drug on *Pf*FKBP35 function
460 in blood stage parasites.

461 In line with our data, previous biochemical approaches revealed potential links between
462 *Pf*FKBP35 and ribosomes. Using co-immunoprecipitation, Leneghan and colleagues revealed
463 that *Pf*FKBP35 is interacting with 480 proteins, of which 31 are ribosomal factors (14). Indeed,
464 FKBP family members are essentially involved in controlling ribosomes in other systems. The
465 human FKBP variant *Hs*FKBP25, for instance, is recruited to the pre-ribosome where its
466 chaperone activity appears to be required for the assembly of the ribosomal large subunit (54).
467 While the FKBP variant of yeast, Fpr4, interacts with the ribosome biogenesis factor Nop53
468 (55), the *Escherichia coli* trigger factor (TF) is part of the ribosomal complex and crucial for
469 the folding of nascent proteins (56, 57). Considering the marked reduction of ribosomal factors
470 in FKBP35$^{\mathbf{KO}}$ parasites, it is tempting to speculate that *Pf*FKBP35 is chaperoning ribosome
471 biogenesis similar to Fpr4 and FKBP25 in *Saccharomyces cerevisiae* and *humans*, respectively.

472 The fact that *Pf*FKBP35 localizes to distinct nuclear foci and its depletion causes dysregulation
473 of ribosomes points towards a role within the nucleolus – the nuclear compartment driving
474 ribosome biogenesis (38). Using IFAs, we found that *Pf*FKBP35 does not co-localize with the
475 nucleolar marker fibrillarin (58) (Fig. S8). However, its localization appears to be intertwined
476 with that of this rRNA methyltransferase. Specifically, *Pf*FKBP35 is mostly found in close
477 vicinity to fibrillarin-rich regions. Nucleoli in eukaryotic cells generally consist of two or, in
478 higher eukaryotes, three sub-compartments. Of those, the granular component (GC) represents
479 the site of pre-ribosome assembly and encompasses fibrillarin-enriched central regions of
480 nucleoli (59). The spatial correlation observed between *Pf*FKBP35 and fibrillarin may thus
481 indicate localization to different sub-nucleolar compartments, with *Pf*FKBP35 occupying the
482 GC area of the nucleolus.

483 In summary, we demonstrate that limiting *Pf*FKBP35 levels are lethal to *P. falciparum* and
484 result in a delayed-death phenotype that is characterized by perturbed ribosome homeostasis
485 and defective protein translation, which is likely linked to the reduced biogenesis of functional
486 ribosomes in the nucleolus. We further show that FKBP-binding drugs, including FK506, exert
487 their parasiticidal activity in a *Pf*FKBP35-independent manner, urging strong caution for the
488 future development of FKBP-targeting antimalarials, especially when based on FK506 and
489 structural derivatives thereof. In addition to revealing first insights into the essential function

490 of *Pf*FKBP35 in ribosome homeostasis of *P. falciparum*, we are convinced that the presented
491 data offer valuable information for target-based efforts in malaria drug discovery.

492

4 Methods

4.1 Parasite culture

P. falciparum culture and synchronization was performed as described (60, 61). Parasites were cultured in AB+ or B+ human red blood cells (Blood Donation Center, Zürich, Switzerland) at a hematocrit of 5% in culture medium containing 10.44 g/L RPMI-1640, 25 mM HEPES, 100 µM hypoxanthine, 24 mM sodium bicarbonate, 0.5% AlbuMAX II (Gibco #11021-037), 0.1 g/L neomycin, and 2 mM choline chloride (Sigma #C7527). To achieve stabilization of DD-tagged proteins in the cell lines NF54/iKD-FKBP35 and NF54/iOE-FKBP35, parasites were cultured in presence of 625 nM Shield-1 (30, 31). To induce the DiCre-mediated recombination of *loxP* sites in NF54/iKO-FKBP35 parasites, cultures were split and treated for 4 h with 100 nM rapamycin or the corresponding volume DMSO, which served as vehicle control, giving rise to $FKBP35^{KO}$ and $FKBP35^{WT}$ populations, respectively (32). Cultures were gassed with 3% O_2, 4% CO_2 and 93% N_2 and incubated in an airtight incubation chamber at 37°C.

4.2 Cloning of transfection constructs

CRISPR/Cas9-based gene editing of the NF54 parasites was performed using a two-plasmid approach as previously described (62, 63). This system is based on co-transfection of a plasmid that contains the expression cassettes for the Cas9 enzyme, the single guide RNA (sgRNA) and the blasticidin deaminase (BSD) resistance marker (pBF-gC), and a pD-derived donor plasmid that contains the template for the homology-directed repair of the Cas9-induced DNA double strand break (Fig. S2A) (63).

The plasmids pBF-gC_FKBP-3', pBF-gC_FKBP-5' and pBF-gC_P230p targeting the 3' or 5' end of *fkbp35* (PF3D7_1247400) or the *p230p* (PF3D7_0208900) locus (64), respectively, were generated by ligation of two annealed oligonucleotides (gRNA_top and gRNA_bottom) into the BsaI-digested pBF-gC backbone (63) using T4 DNA ligase (New England Biolabs).

The donor plasmid pD_FKBP35-iKO was generated by assembling six DNA fragments in a Gibson reaction (65) using (i) the plasmid backbone amplified by polymerase chain reaction (PCR) from pUC19 (primers PCRa_F/PCRa_R) (63), (ii/iii) the 5' and 3' homology regions amplified from genomic DNA (primers PCRb_F/PCRb_R and PCRc_F/PCRc_R, respectively), (iv) the *green fluorescent protein* (*gfp*) sequence amplified from pHcamGDV1-GFP-DD (primers PCRd_F/PCRd_R) (63), (v) the HRPII terminator amplified from genomic DNA (primers PCRe_F/PCRe_R), and (vi) the *fkbp35* sequence containing an artificial *loxPint*

525 (33) amplified from a *P. falciparum* codon-optimized synthetic sequence (primers
526 PCRf_F/PCRf_R) ordered from Genscript.

527 The donor plasmid pD_FKBP35-iKD was generated by assembling five DNA fragments in a
528 Gibson reaction (65) using (i) the plasmid backbone amplified from pUC19 (primers
529 PCRa_F/PCRa_R) (63), (ii/iii) the 5' and 3' homology regions amplified from genomic DNA
530 (primers PCRg_F/PCRg_R and PCRh_F/PCRh_R, respectively), (iv) the *gfp* sequence
531 amplified from pHcamGDV1-GFP-DD (primers PCRi_F/PCRi_R) (63), and (v) the
532 destabilization domain (*dd*) sequence amplified from pHcamGDV1-GFP-DD (primers
533 PCRj_F/PCRj_R) (63).

534 The donor plasmid pD_FKBP35-iOE was generated by assembling three DNA fragments in a
535 Gibson reaction (65) using (i) the NheI/PstI-digested plasmid pkiwi003 (66), (ii) the *fkbp35*
536 coding sequence amplified from genomic DNA (primers PCRk_F/PCRk_R), and (iii) the *gfp-*
537 *dd* sequence amplified from pHcamGDV1-GFP-DD (primers PCRl_F/PCRl_R) (63).

538 Oligonucleotides are listed in Table S4.

539

540 **4.3 Transfection and selection of gene-edited parasites**

541 *P. falciparum* transfection using the CRISPR/Cas9 two-plasmid approach was performed as
542 described previously (63). Briefly, 50 µg of each plasmid (pBF-gC_FKBP-3' and pD_FKBP35-
543 iKO, pBF-gC_FKBP-5' and pD_FKBP35-iKD, pBF-gC_P230p and pD_FKBP35-iOE) were
544 co-transfected into an NF54::DiCre line (67), in which *ap2-g* was tagged with the fluorophore
545 mScarlet as described previously (68). Transgenic parasites were selected with 2.5 µg/mL
546 blasticidin-S-hydrochloride, which was added 24 h after transfection for 10 days. Transgenic
547 populations were usually obtained 2-3 weeks after transfection and correct editing of the
548 modified loci was confirmed by PCR on gDNA (Figs. S1B, S2B and S4B). Primer sequences
549 used for these PCRs are listed in Table S4. Clonal parasite lines were obtained by limiting
550 dilution cloning (69).

551

552 **4.4 DNA content analysis**

553 NF54/iKO-FKBP35 parasites were fixed in 4% formaldehyde/0.0075% glutaraldehyde for 30
554 min at room temperature and washed 3 times in PBS and stored at 4°C. Samples were collected

555 from three independent biological replicates. RNA was digested by incubation with 0.1 mg/mL
556 RNAse A in PBS containing 0.1% Triton-X100 for 15 min at room temperature. Nuclei were
557 stained using 1X SYBR Green 1 DNA stain (Invitrogen S7563) for 20 min and washed three
558 times in PBS. The fixation step quenched the GFP signal detected by the flow cytometer (Fig.
559 S9). SYBR Green intensity was measured using a MACS Quant Analyzer 10 and analyzed
560 using the FlowJo_v10.6.1 software.

561

562 **4.5 Western blotting**

563 Saponin lysis of 500 µL infected red blood cells at 3-5% parasitaemia was performed by
564 incubation for 10 min on ice in 3 mL ice-cold 0.15% saponin in PBS. The parasite pellets were
565 washed two times in ice-cold PBS and resuspended in Laemmli buffer (62.5 mM Tris base, 2%
566 SDS, 10% glycerol and 5% 2-mercaptoethanol). Proteins were separated on 4-12% Bis-Tris
567 gels (Novex, Qiagen) using MOPS running buffer (Novex, Qiagen). Then proteins were
568 transferred to a nitrocellulose membrane (GE healthcare #106000169), which was blocked with
569 5% milk powder in PBS/0.1% Tween (PBS-T) for 1 h. The membrane was probed using the
570 primary antibodies mAb mouse α-GFP (1:1'000, Roche Diagnostics #11814460001), mAb
571 mouse α-*Pf*GAPDH (1:20'000) (70), or mAb mouse α-puromycin (1:5'000, Sigma MABE343)
572 diluted in blocking solution. After 2 h incubation, the membrane was washed 5 times in PBS-
573 T before it was incubated with the secondary antibody goat α-mouse IgG (H&L)-HRP
574 (1:10'000, GE healthcare #NXA931). After 1 h incubation, the membrane was washed 5 times
575 and the signal was detected using the chemiluminescent substrate SuperSignal West Pico Plus
576 (Thermo Scientific, REF 34580) and the imaging system Vilber Fusion FX7 Edge 17.10 SN.
577 Nitrocellulose membranes were stripped by incubating for 10 min in a stripping buffer (1 g/L
578 SDS, 15 g/L glycine, 1% Tween-20, pH 2.2) and washed three times in PBS-T before blocking
579 and re-probing.

580

581 **4.6 Drug dose-response experiments**

582 Dose-response relationships were assessed by exposing synchronous ring stage parasites at
583 0.5% parasitaemia and 1.25% hematocrit to 12 drug concentrations using a two-step serial
584 dilution in 96-well plates (Corning Incorporated, 96-well cell culture plate, flat bottom, REF
585 3596) in three independent biological replicates. The plates were gassed and incubated for 48
586 h at 37 °C. FK506 (MedChemExpress HY-13756), D44 (ChemBridge 7934155 and ChemDiv

587 7286-2836) and cyclosporin A (Sigma 30024) stocks of 10 mM were prepared in DMSO and
588 working solutions were prepared immediately before the experiment. To measure parasite
589 survival using flow cytometry, cultures were stained in 1X SYBR Green 1 DNA stain
590 (Invitrogen S7563) in a new 96-well plate (Corning Incorporated, 96-well cell culture plate,
591 round bottom, REF 3788) and incubated in the dark for 20 min. The samples were washed once
592 in PBS. Using a MACS Quant Analyzer 10, 50'000 events per condition were measured and
593 analyzed using the FlowJo_v10.6.1 software. Infected RBCs were identified based on SYBR
594 Green 1 DNA stain intensity. The gating strategy is shown in Fig. S9. To quantify parasite
595 survival based on hypoxanthine incorporation into DNA, compounds were dissolved in DMSO (10
596 mM), diluted in hypoxanthine-free culture medium and titrated in duplicates over a 64-fold range (6 step
597 twofold dilutions) in 96 well plates. 100 µl asexual parasite culture (prepared in hypoxanthine-free
598 medium) were added to each well and mixed with the compound to obtain a final haematocrit of 1.25%
599 and a final parasitemia of 0.3%. After incubation for 48 hrs, 0.25 µCi of [3H]-hypoxanthine was added
600 per well and plates were incubated for an additional 24 hrs. Parasites were then harvested onto glass-
601 fiber filters using a Microbeta FilterMate cell harvester (Perkin Elmer, Waltham, US) and radioactivity
602 was counted using a MicroBeta2 liquid scintillation counter (Perkin Elmer, Waltham, US). The results
603 were recorded and expressed as a percentage of the untreated controls. Curve fitting and IC50
604 calculations were performed using a non-linear, four-parameter regression model with variable
605 slope (Graph Pad Prism, version 8.2.1).

606

607 **4.7 Fluorescence microscopy**

608 To localize *Pf*FKBP35, NF54/iKD-FKBP35 parasites were fixed in 4% formaldehyde/0.0075%
609 glutaraldehyde for 30 min at room temperature and washed three times in PBS. The fixed cells
610 were permeabilized by incubation with 0.1% Triton-X100-containing PBS for 15 min. After
611 two washing steps in PBS, the cells were incubated in a blocking/aldehyde quenching solution
612 (3% BSA in PBS complemented with 50 mM ammonium chloride). The samples were
613 incubated with the primary antibodies rabbit α-GFP (1:400, Abcam ab6556) and mAb mouse
614 α-fibrillarin (1:100, Santa Cruz Biotechnology sc-166021) for 1 h in 3% BSA in PBS and
615 washed 3 times in PBS. Subsequently, the samples were incubated with the secondary
616 antibodies goat α-rabbit IgG (H&L) Alexa Fluor 488 (1:250, Invitrogen A11008) and goat a-
617 mouse IgG (H&L) Alexa Fluor 594 (1:250, Invitrogen A11032), for 1 h and washed 3 times,
618 before they were mixed with Vectashield containing DAPI (Vector laboratories, H-1200), and

619 mounted on a microscopy slide. Slides were imaged using a Leica THUNDER 3D Assay
620 imaging system.

621

622 **4.8 Proteomics**

623 Parasite cultures were split at 0-6 hpi in G1 and treated for 4 h with 100 nM rapamycin. Saponin
624 lysis of paired FKBP35^{WT} and FKBP35^{KO} populations at 36-42 hpi in G1 and 24-30 hpi in G2
625 was performed as described above. Samples were collected in three independent biological
626 replicates. The washed parasite pellet was snap frozen in liquid nitrogen. After thawing,
627 parasites were resuspended in 25 µL of lysis buffer (5% SDS, 100 mM tetraethylammonium
628 bromide (TEAB), 10 mM tris(2-carboxyethyl)phosphin (TCEP), pH 8.5) and sonicated (10
629 cycles, 30 sec on/off at 4 °C, Bioruptor, Diagnode). Lysates were subsequently reduced for 10
630 minutes at 95 °C. Samples were then cooled down to RT and 0.5 µL of 1M iodoacetamide was
631 added to the samples. Cysteine residues were alkylated for 30 min at 25 °C in the dark.
632 Digestion and peptide purification was performed using S-trap technology (Protifi) according
633 to the manufacturer's instructions. In brief, samples were acidified by addition of 2.5 µL of
634 12% phosphoric acid (1:10) and then 165 µL of S-trap buffer (90% methanol, 100 mM TEAB
635 pH 7.1) was added to the samples (6:1). Samples were briefly vortexed and loaded onto S-trap
636 micro spin-columns (Protifi) and centrifuged for 1 min at 4000 g. Flow-through was discarded
637 and spin-columns were then washed 3 times with 150 µL of S-trap buffer (each time samples
638 were centrifuged for 1 min at 4000 g and flow-through was removed). S-trap columns were
639 then moved to the clean tubes and 20 µL of digestion buffer (50 mM TEAB pH 8.0) and trypsin
640 (at 1:25 enzyme to protein ratio) were added to the samples. Digestion was allowed to proceed
641 for 1h at 47 °C. Then, 40 µL of digestion buffer were added to the samples and the peptides
642 were collected by centrifugation at 4000 g for 1 minute. To increase the recovery, S-trap
643 columns were washed with 40 µL of 0.2% formic acid in water (400g, 1 min) and 35 µL of
644 0.2% formic acid in 50% acetonitrile. Eluted peptides were dried under vacuum and stored at -
645 20 °C until further analysis.

646 Peptides were resuspended in 0.1% aqueous formic acid and peptide concentration was adjusted
647 to 0.25 µg/µL. 1 µL of each sample was subjected to LC-MS/MS analysis using an Orbitrap
648 Elicpse Tribrid Mass Spectrometer fitted with an Ultimate 3000 nano system (both from
649 Thermo Fisher Scientific) and a custom-made column heater set to 60 °C. Peptides were
650 resolved using a RP-HPLC column (75 µm × 30 cm) packed in-house with C18 resin (ReproSil-

651 Pur C18–AQ, 1.9 µm resin; Dr. Maisch GmbH) at a flow rate of 0.3 µL/min. The following
652 gradient was used for peptide separation: from 2% buffer B to 12% B over 5 min, to 30% B
653 over 40 min, to 50% B over 15 min, to 95% B over 2 min followed by 11 min at 95% B then
654 back to 2% B. Buffer A was 0.1% formic acid in water and buffer B was 80% acetonitrile, 0.1%
655 formic acid in water.

656 The mass spectrometer was operated in DDA mode with a cycle time of 3 seconds between
657 master scans. Each master scan was acquired in the Orbitrap at a resolution of 240,000 FWHM
658 (at 200 m/z) and a scan range from 375 to 1600 m/z followed by MS2 scans of the most intense
659 precursors in the linear ion trap at "Rapid" scan rate with isolation width of the quadrupole set
660 to 1.4 m/z. Maximum ion injection time was set to 50 ms (MS1) and 35 ms (MS2) with an AGC
661 target set to 1e6 and 1e4, respectively. Only peptides with charge state 2-5 were included in the
662 analysis. Monoisotopic precursor selection (MIPS) was set to Peptide, and the Intensity
663 Threshold was set to 5e3. Peptides were fragmented by HCD (Higher-energy collisional
664 dissociation) with collision energy set to 35%, and one microscan was acquired for each
665 spectrum. The dynamic exclusion duration was set to 30 seconds.

666 The acquired raw-files were imported into the Progenesis QI software (v2.0, Nonlinear
667 Dynamics Limited), which was used to extract peptide precursor ion intensities across all
668 samples applying the default parameters. The generated mgf-file was searched using MASCOT
669 against a *Plasmodium falciparum* (isolate 3D7) database (Uniprot, 11.2019) and 392 commonly
670 observed contaminants using the following search criteria: full tryptic specificity was required
671 (cleavage after lysine or arginine residues, unless followed by proline); 3 missed cleavages were
672 allowed; carbamidomethylation (C) was set as fixed modification; oxidation (M) and acetyl
673 (Protein N-term) were applied as variable modifications; mass tolerance of 10 ppm (precursor)
674 and 0.6 Da (fragments). The database search results were filtered using the ion score to set the
675 false discovery rate (FDR) to 1% on the peptide and protein level, respectively, based on the
676 number of reverse protein sequence hits in the dataset. Quantitative analysis results from label-
677 free quantification were processed using the SafeQuant R package v.2.3.2 (71) to obtain peptide
678 relative abundances. This analysis included global data normalization by equalizing the total
679 peak/reporter areas across all LC-MS runs, data imputation using the knn algorithm, summation
680 of peak areas per protein and LC-MS/MS run, followed by calculation of peptide abundance
681 ratios. Only isoform specific peptide ion signals were considered for quantification. To meet
682 additional assumptions (normality and homoscedasticity) underlying the use of linear
683 regression models and t-Tests, MS-intensity signals were transformed from the linear to the

684 log-scale. The summarized peptide expression values were used for statistical testing of
685 between condition differentially abundant peptides. Here, empirical Bayes moderated t-Tests
686 were applied, as implemented in the R/Bioconductor limma package (72). The resulting per
687 protein and condition comparison *p*-values were adjusted for multiple testing using the
688 Benjamini-Hochberg method.

689 Gene ontology enrichment analysis was performed using the PANTHER Overrepresentation
690 Test with the correction method "False Discovery Rate", the test type "Fisher's Exact", and the
691 annotation data set "PANTHER GO-Slim" (37).

692

693 **4.9 IPP complementation**

694 Parasite cultures were split at 0-6 hpi in G1 and treated for 4 h with 100 nM rapamycin.
695 FKBP35^{KO} and FKBP35^{WT} populations were split again and supplemented either with 200 µM
696 isopentenyl pyrophosphate (IPP) (Sigma I0503) or the corresponding volume H_2O. The
697 respective culture medium was replaced daily. Parasites treated with 156 ng/mL doxycycline
698 (Sigma D9891) were used to confirm that IPP complementation is able to rescue apicoplast-
699 deficient parasites. DNA content analysis was performed as described above.

700

701 **4.10 Heat shock susceptibility testing**

702 Parasites cultures were split at 0-6 hpi in G1 and treated for 4 h with 100 nM rapamycin. While
703 control populations were always incubated at 37 °C, test populations were incubated at 40 °C
704 for 6 h starting at 24-30 hpi. Parasitaemia was measured in G2 using flow cytometry as
705 described above.

706

707 **4.11 Surface sensing of translation (SUnSET)**

708 Parasite cultures were split at 0-6 hpi in G1 and treated for 4 h with 100 nM rapamycin. At 24-
709 30 hpi in G2, the cultures were incubated with 1 µg/mL puromycin (Sigma P8833) for 1 h at
710 37 °C (40, 73). Saponin lysis and Western blotting were performed as described above.

711

712 ### 4.12 Cellular thermal shift assay (CETSA)

713 The mass spectrometry-based isothermal dose-response cellular thermal shift assay (ITDR-MS-
714 CETSA) was performed according to the protocol developed by Dziekan and colleagues (48).
715 Briefly, live parasites (10^7 MACS-purified trophozoites per condition) were exposed to a
716 FK506 (MedChemExpress HY-13756) concentration gradient (100 µM to 1.5 nM) and a
717 DMSO control for 1 h. Subsequently, the parasites were washed in PBS and exposed to the
718 denaturing temperatures 50 °C, 55 °C and 60 °C as well as to a non-denaturing temperature 37
719 °C for 3 min, before they were cooled down to 4 °C for 3 min. Afterwards, the cells were lysed
720 by resuspending in a lysis buffer (50 mM HEPES pH 7.5, 5 mM β-glycerophosphate, 0.1 mM
721 Na_3VO_4, 10 mM $MgCl_2$, 2 mM TCEP, and EDTA-free protease inhibitor cocktail (Sigma)),
722 three freeze/thaw cycles, and mechanical shearing using a syringe with a 31-gauge needle.
723 Subsequently, insoluble proteins were pelleted by centrifugation (20 min at 4 °C and 20'000 g)
724 and the soluble fraction was collected and subjected to protein digestion, reduction, alkylation,
725 and TMT10 labelling followed by LC/MS analysis as described (48).

726 To prepare the protein lysate, saponin-lysed parasites were lysed in the afore-mentioned buffer
727 by three freeze/thaw cycles and mechanical shearing. After centrifugation, soluble proteins
728 were exposed to a FK506 concentration gradient (200 µM to 3 nM) and a DMSO control for 1
729 min before the thermal challenge was performed as described above. Afterwards, the soluble
730 protein fraction was isolated and prepared for by LC/MS analysis as described (48).

731 Data analysis was performed using the Proteome Discoverer 2.1 software (Thermo Fisher
732 Scientific) and the R package "mineCETSA" (v 1.1.1). Only proteins identified by at least three
733 peptide spectrum matches (PSMs) were included in the analysis (48).

734

735 ### 4.13 Transcriptomics

736 #### 4.13.1 Sample preparation

737 The RNA of 500 µL iRBCs at 3-5% parasitaemia was isolated using 3 mL TRIzol reagent
738 (Invitrogen) followed by purification using the Direct-zol RNA MiniPrep kit (Zymo). Samples
739 were collected from three biological replicates. Stranded RNA sequencing libraries were
740 prepared using the Illumina TruSeq stranded mRNA library preparation kit (REF 20020594)
741 according to the manufacturer's protocol. The library was sequenced in 100 bp paired-end reads

742 on an Illumina NextSeq 2000 sequencer using the Illumina NextSeq 2000 P3 reagents (REF
743 20040560), resulting in 5 million reads on average per sample.

744 **4.13.2 RNA-Seq data analysis**

745 Fastqc was run on all raw fastq files. Then, each file was aligned with hisat2 (version 2.0.5)
746 (74) against the 3D7 reference genome (PlasmoDB v58) (75) in which the GFP and the recoded
747 FBPK35 sequences were added at the end of chromosome 12. Read counts for each gene and
748 for each sample were then counted using featureCount (gff file from PlasmoDB v58 modified
749 to include the added GFP and FBPK35). TPM (Transcripts Per Kilobase Million) were then
750 calculated from the raw count matrix.

751 Principal component analysis (PCA) was performed using the R (version 4.2.1) function
752 prcomp using log transformed TPMs. PCA revealed that the rapamycin-treated replicate B of
753 TP 3 ("3B.R") was a clear outlier and is different from any other replicate at any time point
754 (Fig. S3D). For this reason, it was excluded from further analysis. The PCA was done again
755 without it and the other samples show the same pattern as the initial PCA (Fig. S3E).

756 DESeq2 (version 1.36) (76) was used for normalization and differential expression analysis.
757 Paired differential expression tests where done for each time point using DESeq2 LRT
758 (likelihood ratio test) using the full model ~ Treatment + Replicate (Treatment is DMSO or
759 Rapamycin and Replicate is the clone, added as the data is paired) and the reduced model ~
760 Replicate. From this paired test and the average log fold-change calculated from the TPMs,
761 normalized volcano plots were made using the R package EnhancedVolcano (version 1.14)
762 (77).

763 **4.13.3 Cell cycle analysis**

764 Spearman correlation between normalized scaled read counts for each sample for all genes (as
765 one vector) and each time point of the reference microarray time course published by Bozdech
766 *et al*. (41) (3D7 smoothed, retrieved from PlasmoDB) were tested. Spearman's coefficients rho
767 for each time point of this RNA-Seq time course and each time point of the reference data set
768 where plotted using ggcorrplot (version 0.1.3) (78). For each time point of this RNA-Seq
769 dataset, the rho coefficients where then plotted against the time points of the reference data set
770 and the FKBP35^{WT} and FKBP35^{KO} data were fitted separately to the linearized sinusoidal $A *$
771 $sin\left(\frac{2\pi}{53}time\right) + B * cos\left(\frac{2\pi}{53}time\right) + C$ using R lm function. The time point matching best to
772 the FKBP35$^{\mathbf{WT}}$ and FKBP35$^{\mathbf{KO}}$ samples for each time point of the RNA-Seq time course was

taken as the maximum of this fitted function. Both fitted functions were F-tested (using R function var.test using both fitted model as applied to the FKBP35^{KO} data) to test whether the FKBP35^{WT} and FKBP35^{KO} data correlated with the reference data set (41) in a significantly different way, which would indicate a cell cycle shift if statistically significant. Only the last time point showed such a significant difference.

Data availability

The mass spectrometry proteomics data have been deposited to the ProteomeXchange Consortium repository with the dataset identifier PXD039018. The sequencing data are available in the Sequence Read Archive (SRA) via the accession number PRJNA914079.

Acknowledgements

We thank Vera Mitesser and Ron Dzikowski for guidance on the SUnSET experiments and David Fidock for providing the parasite line Dd2-B2 used for the attempted resistance selection. We are grateful to the Polyomics facility at the University of Glasgow for processing the samples for RNA-Seq. This work was supported by the Swiss National Foundation (grant number 310030_200683), the Wolfson Merit Royal Society Award, the Wellcome Trust Investigator Award 110166 and Wellcome Trust Center Award 104111, and by the Singapore Ministry of Education (grant number MOE-T2EP30120-0015).

Author contributions

B.T.T. designed and performed experiments, analyzed and interpreted the data, and wrote the original draft of the manuscript. J.M.D. and S.T. performed and interpreted CETSA experiments. Z.B. supervised these experiments and provided resources. F.A. analyzed RNA-Seq data. M.M. supervised these experiments and provided resources for RNA-Seq data generation. A.P. performed immunofluorescence assays. K.B. performed and analyzed proteomics experiments supervised by A.S. C.Gu. and M.R. performed and interpreted hypoxanthine incorporation assays. C.Gr. edited the manuscript. N.M.B.B. conceived the study, designed and supervised experiments, provided resources, and wrote the manuscript. All authors contributed to the final editing of the manuscript.

Declaration of interests

The authors declare that they have no conflict of interest.

807 **Figures**

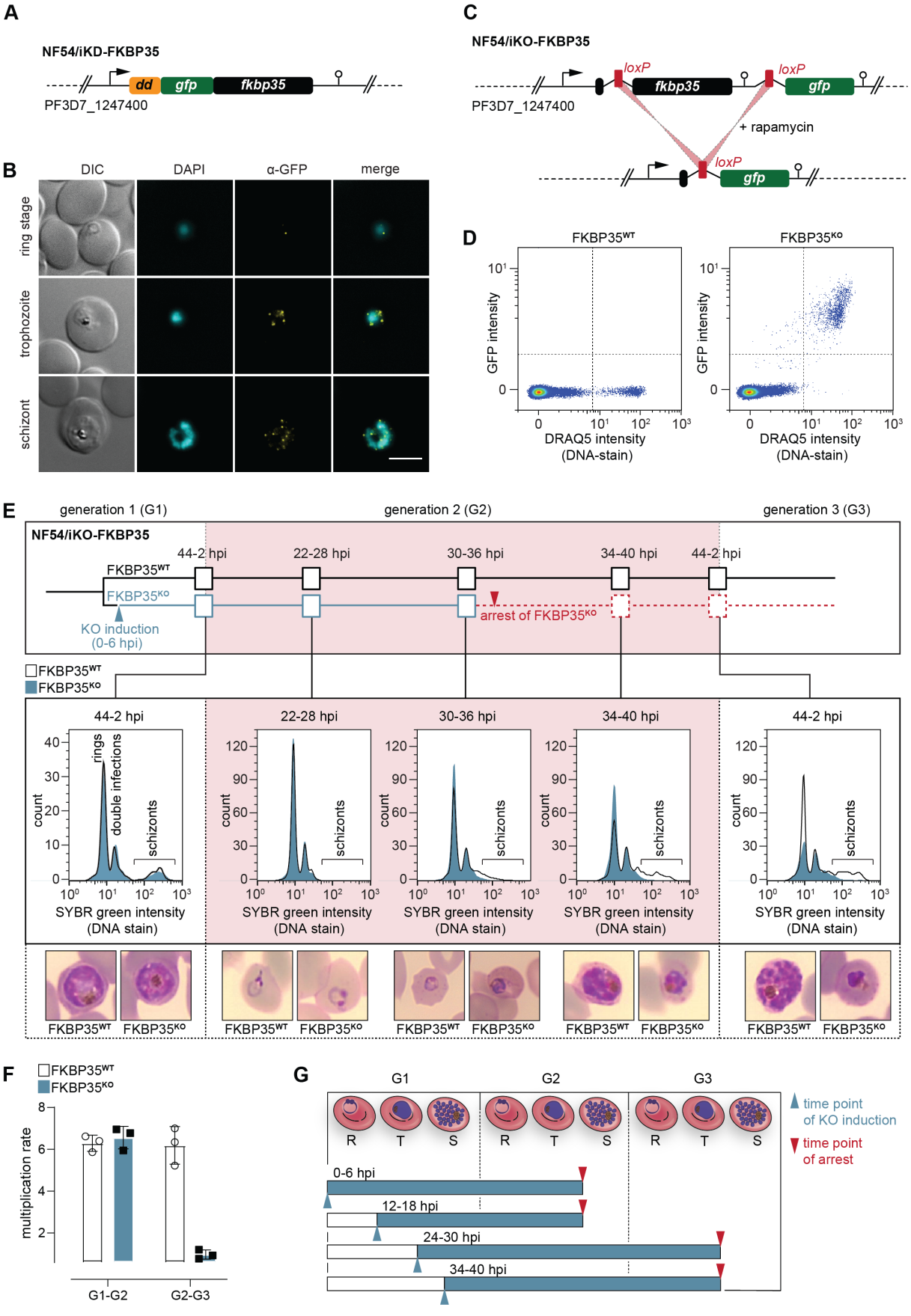

808

809

810 **Figure 1. *Pf*FKBP35 depletion causes delayed parasite death.**

811 **(A)** Schematic of the N-terminally modified *fkbp35* locus in NF54/iKD-FKBP35 parasites. *dd*,
812 destabilization domain. *gfp*, *green fluorescent protein*. **(B)** Localization of *Pf*FKBP35 in
813 NF54/iKD-FKBP35 parasites at the ring, trophozoite and schizont stage assessed by
814 immunofluorescence. DNA was stained with DAPI. Representative images are shown. Scale
815 bar: 5 µm. DIC, differential interference contrast.**(C)** Schematic of the modified *fkbp35* locus
816 in NF54/iKO-FKBP35 parasites before and after *loxP* recombination. *gfp*, *green fluorescent*
817 *protein*. **(D)** Flow cytometry plot showing GFP expression in G1 schizonts of FKBP35$^{\mathbf{KO}}$ and
818 FKBP35$^{\mathbf{WT}}$. DNA was stained with DRAQ5. **(E)** Time course showing the development of
819 NF54/iKO-FKBP35 parasites. Upper panel: Schematic of the experimental setup. Middle
820 panel: DNA content of the populations assessed by flow cytometry based on the SYBR Green
821 intensity. Lower panel: Giemsa-stained blood smears. The knockout was induced at 0-6 hpi.
822 Representative data of three biological replicates are shown. **(F)** Multiplication rates of
823 FKBP35$^{\mathbf{KO}}$ and FKBP35$^{\mathbf{WT}}$ parasites from generation 1 to generation 2 (G1-G2) and G2-G3.
824 The knockout was induced at 0-6 hpi. Multiplication rates were determined using flow
825 cytometry. Data points represent the multiplication rates from G1-G2 and G2-G3. n=3, error
826 bars represent the standard error of the mean. **(G)** Schematic showing time point of growth
827 arrest (red arrow) following *Pf*FKBP35 knock-out at different hpi (blue arrow). R, ring stage;
828 T, trophozoite stage; S, schizont stage.

829

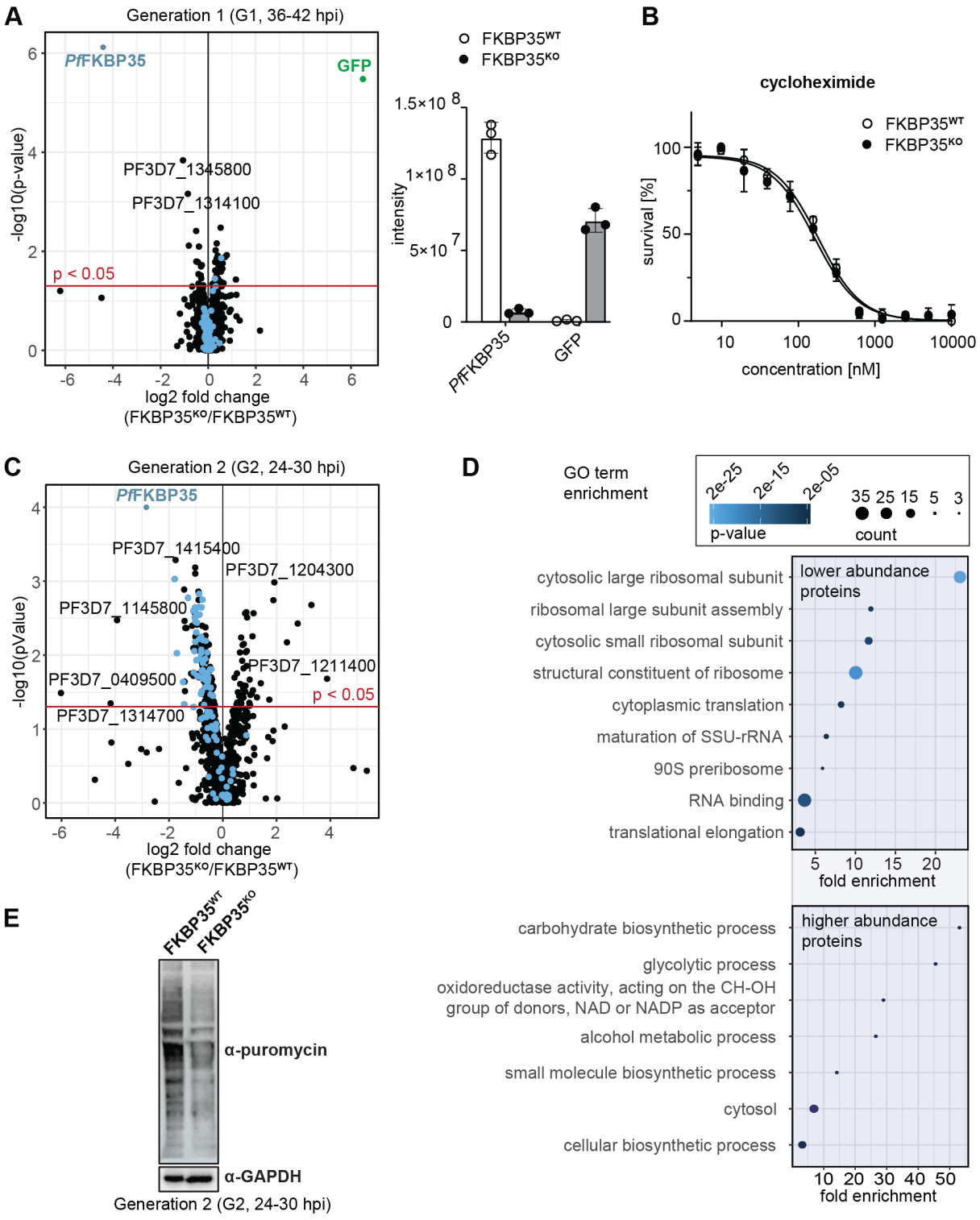

Figure 2. *Pf*FKBP35 is crucial for ribosome homeostasis and protein translation.

(A) Left panel: Proteome analysis of schizonts (36-42 hpi) in G1. The volcano plot shows change in protein abundance in FKBP35^{KO} compared to FKBP35^{WT}. Ribosomal proteins are highlighted in blue, n=3. Right panel: Relative difference in *Pf*FKBP35 and GFP abundance expressed as signal intensity measured by mass spectrometry. n=3, error bars represent the standard error of the mean. **(B)** Dose-response effect of the translation inhibitor cycloheximide

837 on FKBP35^{KO} and FKBP35^{WT} parasites. The knockout was induced at 0-6 hpi and parasites
838 were subsequently exposed to cycloheximide for 48 h. Parasite survival was quantified by flow
839 cytometry. n=3, error bars represent the standard error of the mean. **(C)** Proteome analysis of
840 trophozoites (24-30 hpi) in G2. The volcano plot shows change in protein abundance in
841 FKBP35^{KO} compared to FKBP35^{WT}. Ribosomal proteins are highlighted in blue. n=3. **(D)** GO
842 enrichment analysis of significantly deregulated proteins in FKBP35^{KO} trophozoites in G2. GO
843 enrichment analysis was performed using the PANTHER "Overrepresentation Test" with the
844 test type "Fisher's Exact" and the correction method "False Discovery Rate". **(E)** Assessment
845 of translation activity using SUnSET. FKBP35^{KO} and FKBP35^{WT} trophozoites of G2 were
846 incubated with puromycin for 1 hour. Incorporated puromycin was detected using an α-
847 puromycin antibody. α-GAPDH served as loading control. n=3, a representative Western blot
848 is shown.
849

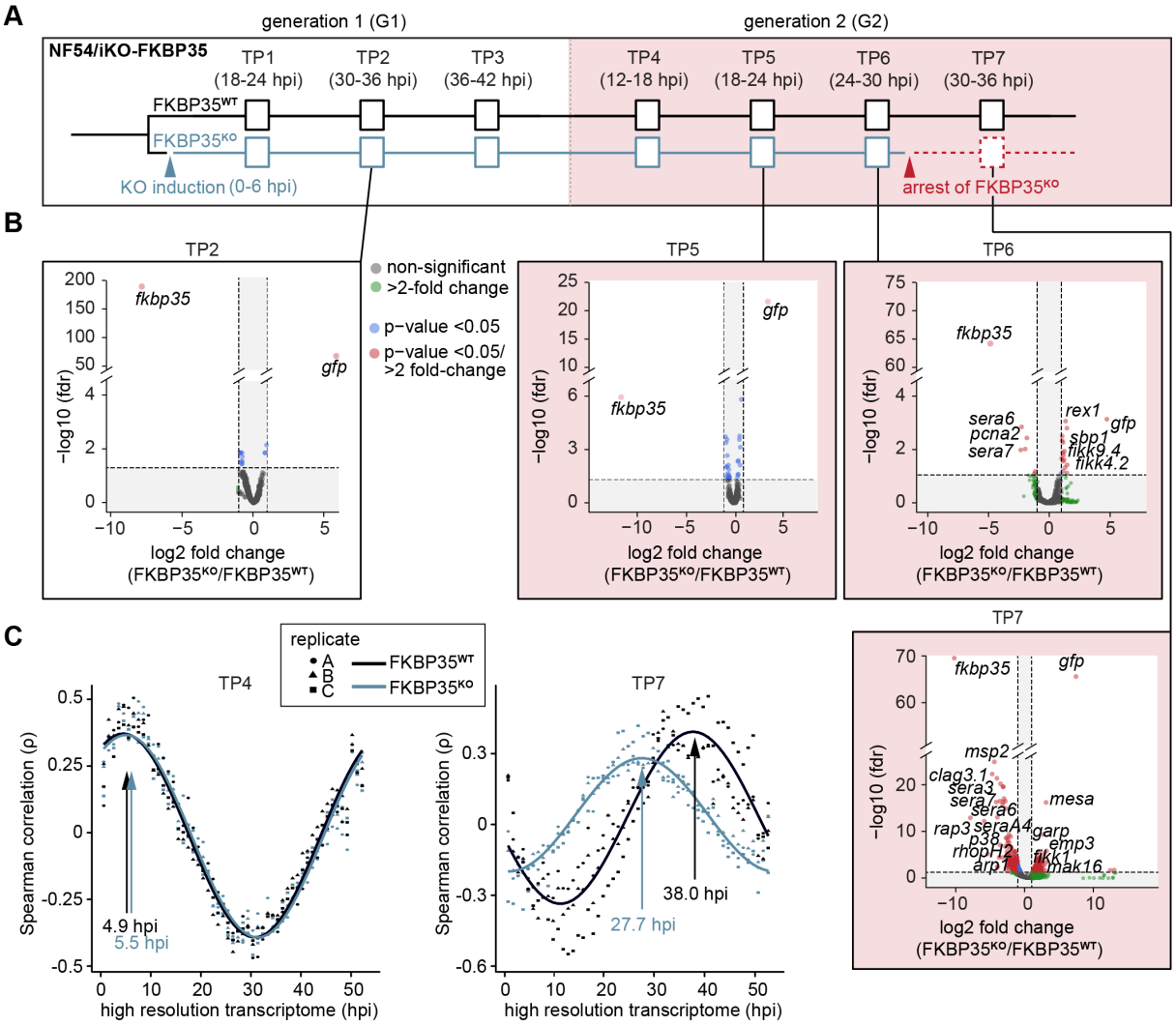

Figure 3. The knockout of *Pf*FKBP35 remains silent at the transcriptomic level.

(A) Setup of the RNA-Seq experiment. RNA was collected at seven indicated time points (TP). **(B)** Volcano plots show differential gene expression between FKBP35^{KO} and FKBP35^{WT} parasites. Genes are color-coded according to the fold change and fdr (false discovery rate), n=3. **(C)** Mapping of FKBP35^{KO} and FKBP35^{WT} transcriptomes to a high-resolution reference (41). Spearman rank coefficients (ρ) show correlation between the sampled transcriptomes and the reference data set (41). The time points with the highest correlation coefficient are indicated.

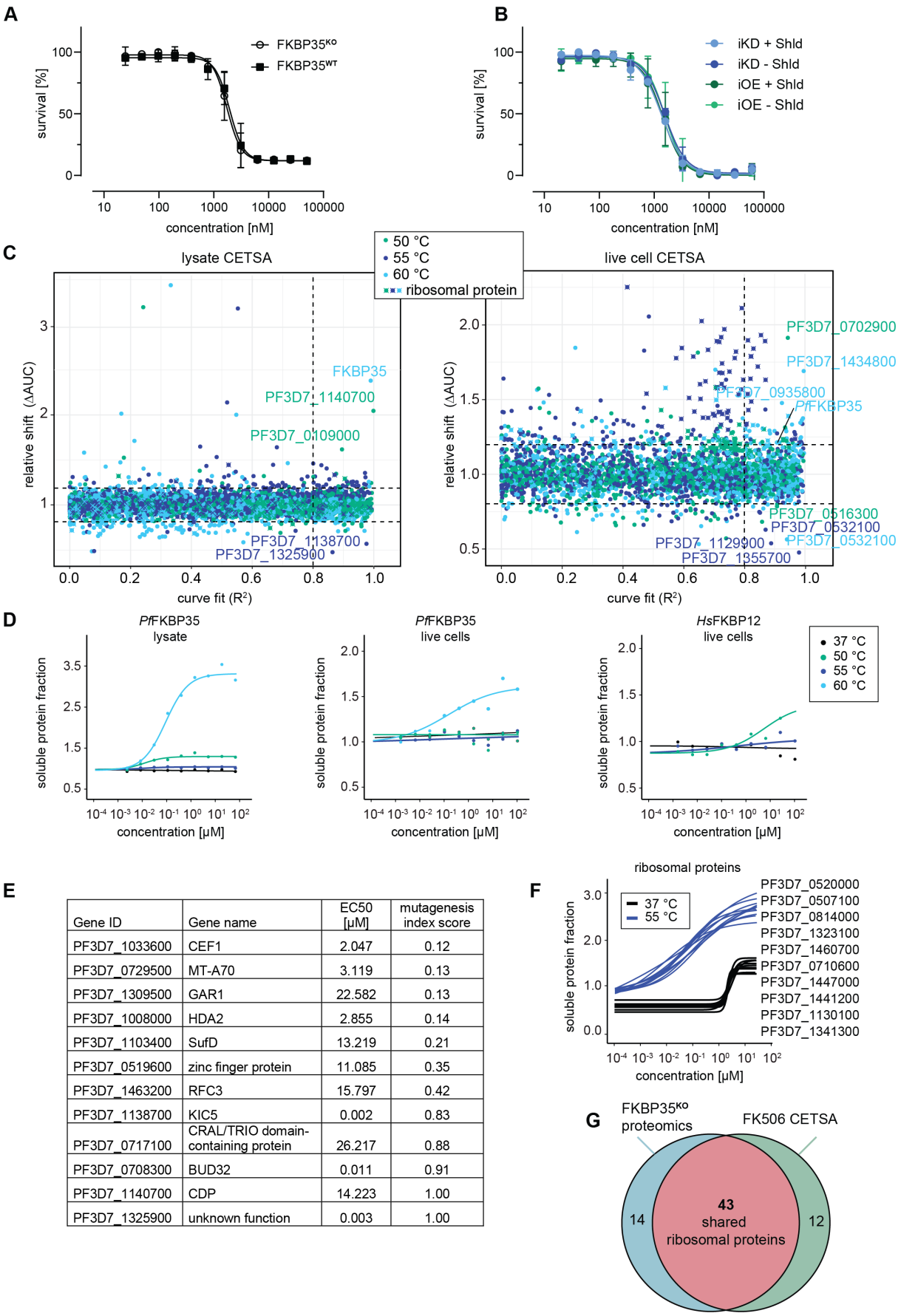

Gene ID	Gene name	EC50 [µM]	mutagenesis index score
PF3D7_1033600	CEF1	2.047	0.12
PF3D7_0729500	MT-A70	3.119	0.13
PF3D7_1309500	GAR1	22.582	0.13
PF3D7_1008000	HDA2	2.855	0.14
PF3D7_1103400	SufD	13.219	0.21
PF3D7_0519600	zinc finger protein	11.085	0.35
PF3D7_1463200	RFC3	15.797	0.42
PF3D7_1138700	KIC5	0.002	0.83
PF3D7_0717100	CRAL/TRIO domain-containing protein	26.217	0.88
PF3D7_0708300	BUD32	0.011	0.91
PF3D7_1140700	CDP	14.223	1.00
PF3D7_1325900	unknown function	0.003	1.00

Figure 4. CETSA identifies FK506 interaction partners.

861 **(A)** Dose-response effect of FK506 on FKBP35^{KO} and FKBP35^{WT} parasites. The knockout was
862 induced at 0-6 hpi and parasites were exposed to FK506 for 48h. n=3, error bars represent the
863 standard error of the mean. **(B)** Dose-response effect of FK506 on NF54/iKD-FKBP35 and
864 NF54/iOE-FKBP35 parasites in presence and absence of Shield-1 (Shld). Parasites were split
865 at 0-6 hpi and subsequently treated with Shld or the vehicle control EtOH. Data points represent
866 the mean of three and two independent biological replicates for the NF54/iOE-FKBP35 and
867 NF54/iKD-FKBP35 cell line, respectively. Error bars represent the standard error of the mean.
868 **(C)** CETSA results. The relative shift in protein abundance (area under the curve of heat-
869 challenged samples normalized against the non-denaturing control, ΔAUC) as a function of R^2
870 (goodness of fit as a measure for the dose-response effect). The dashed lines indicate an
871 arbitrary cutoff of 3 times the median absolute deviation (MAD) of each dataset and R^2=0.8.
872 Three different temperatures were used for protein denaturation (indicated by colors). **(D)** Dose-
873 dependent stabilization of *P. falciparum* and human FKBPs detected using lysate and live cell
874 CETSA. Bullets represent the abundance of non-denatured proteins in response to increasing
875 FK506 concentrations under thermal challenge relative to the DMSO control. Colors indicate
876 the temperatures used for heat challenge; the black curve represents the non-denaturing (37°C)
877 control. **(E)** Proteins with the most pronounced stability shift under thermal challenge in the
878 lysate CETSA experiment are listed. The EC50 is the concentration at which the half-maximal
879 effect of the FK506-induced thermal stabilization is reached. The mutagenesis index score
880 determined by Zhang *et al*. (18) is a measure to predict if a protein is essential for asexual
881 growth: 0=essential, 1=non-essential. **(F)** Fitted live cell CETSA curves of 10 representative
882 ribosomal proteins at 37°C and 55°C. Ribosomal proteins show a FK506 dose-dependent
883 increase in soluble protein fraction. **(G)** Venn diagram showing the overlap between ribosomal
884 proteins deregulated in the *Pf*FKBP35 knock-out cell line (less abundant in G2 FKBP^{KO}
885 trophozoites determined by proteomics) and the ribosomal proteins stabilized by FK506 in live
886 cell CETSA. The number of factors identified in either or both assays is indicated.
887

888 **Supplemental figures**

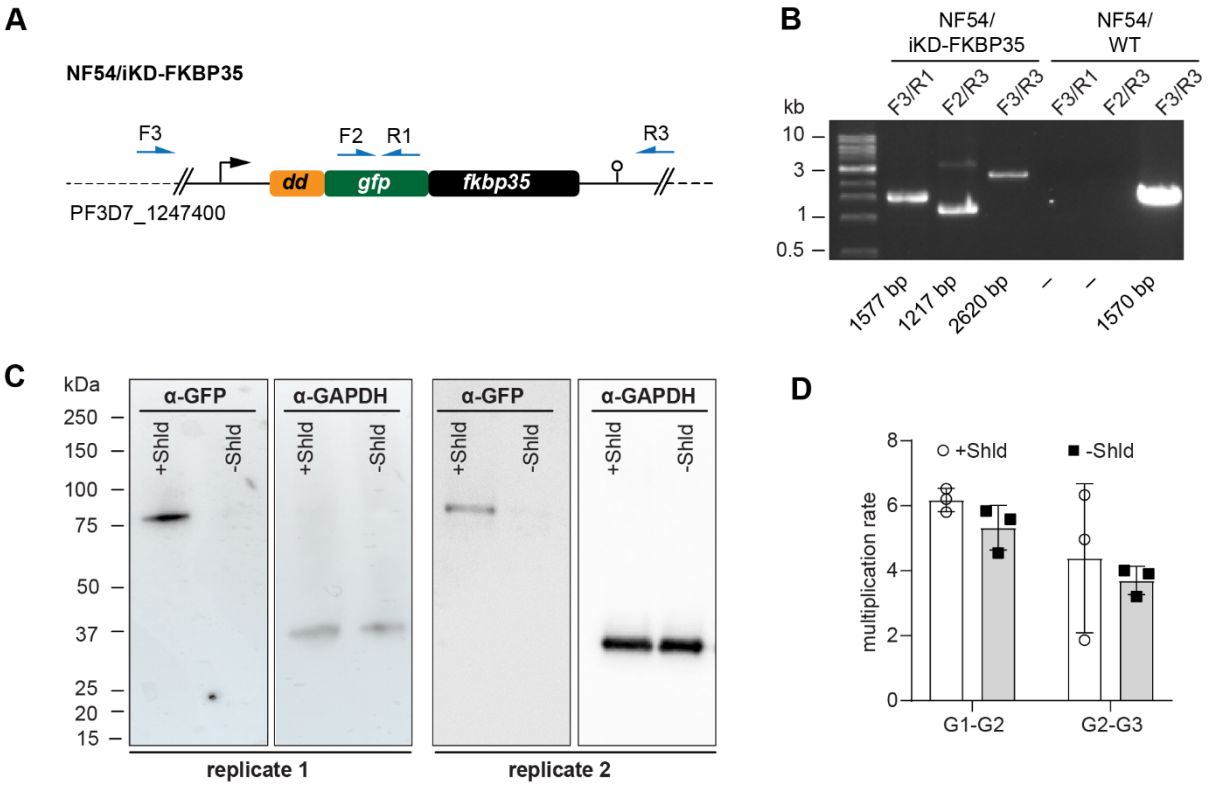

889

890 **Figure S1. Characterization of NF54/iKD-FKBP35 parasites.**

891 **(A)** Schematic of the modified *fkbp35* locus (PF3D7_1247400) in NF54/iKD-FKBP35
892 parasites. The 5'-end of *fkbp35* was tagged with the sequences of a destabilization domain (*dd*)
893 and a green fluorescent protein (*gfp*). The DD tag allows regulating protein levels post-
894 translationally using the stabilizing compound Shield-1 (Shld) (30, 31). Names and binding
895 sites of the primers used for diagnostic PCRs are indicated. **(B)** Diagnostic PCRs performed on
896 gDNA of NF54/FKBP35 iKD parasites to confirm correct editing of the locus. PCRs performed
897 on NF54/WT gDNA served as control. Numbers at the bottom indicate expected fragement
898 sizes. **(C)** Expression levels of the DD-GFP-FKBP35 fusion protein were assessed by Western
899 blot. Parasite cultures were split at 0-6 hpi and treated with Shld or the vehicle control EtOH.
900 Protein lysates were collected 40 hours later. α-GAPDH served as loading control. The expected
901 size of the DD-GFP-FKBP35 fusion protein is 74.2 kDa. **(D)** Multiplication rates of NF54/iKD-
902 FKBP35 parasites from generation 1 to generation 2 (G1-G2) and G2-G3. Parasites were split
903 at 0-6 hpi and treated with Shld or the vehicle control EtOH. Multiplication rates were
904 determined using flow cytometry. Data points represent the multiplication rates from G1-G2
905 and G2-G3, respectively. n=3; error bars represent the standard error of the mean.

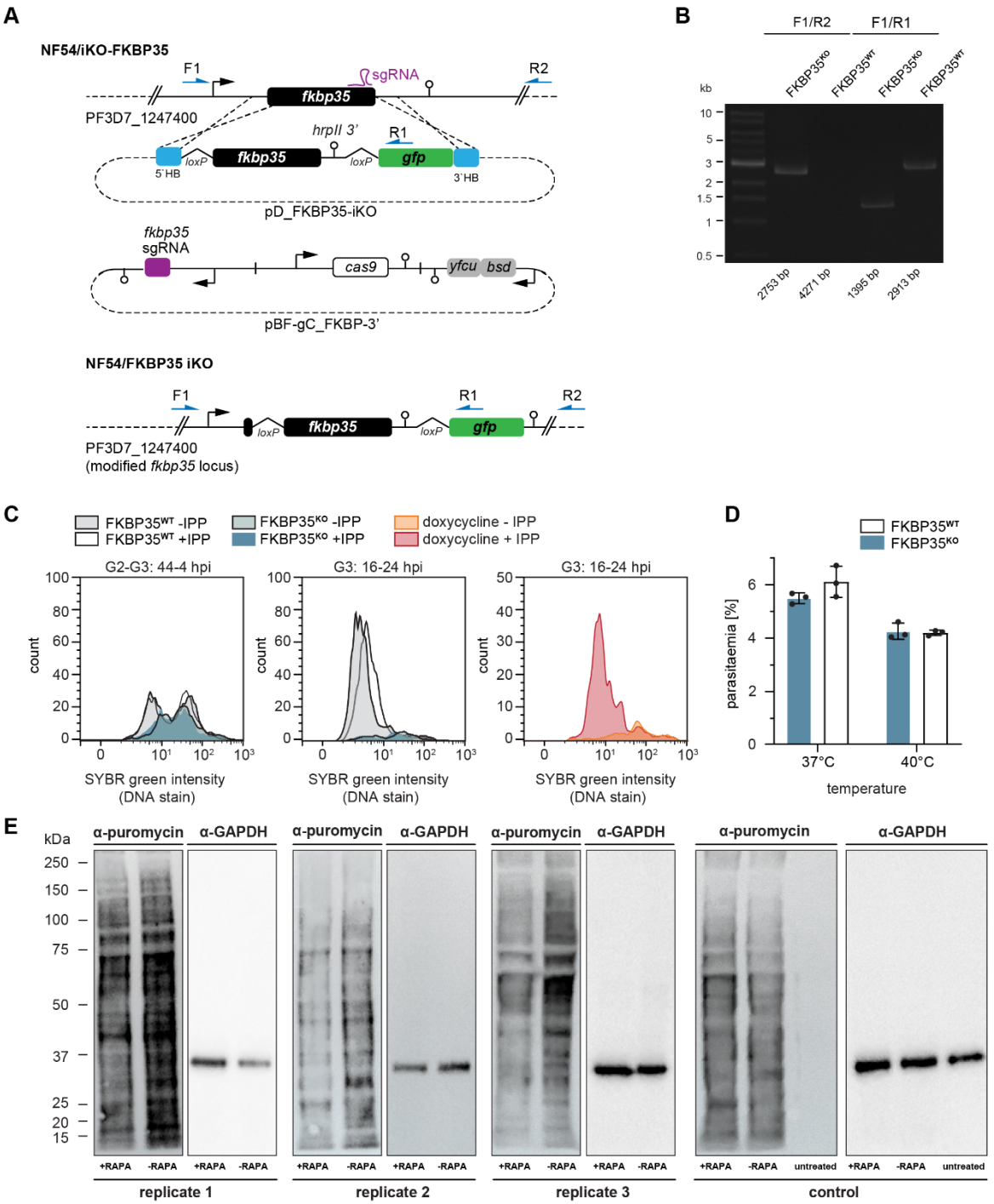

Figure S2. CRISPR/Cas9-based generation of transgenic parasite lines.

(A) Schematic of the wild type *fkbp35* locus (PF3D7_1247400) and the two plasmids used for CRISPR/Cas9 gene editing (pD_FKBP35-iKO and pBF-gC_FKBP-3') to generate the modified *fkbp35* locus of NF54/iKO-FKBP35 parasites. The modification consists of an intron containing a *loxP* site that was introduced after the first 38 bp of the coding sequence and an *hrpII* terminator inserted after the stop codon followed by another *loxP* site and a *gfp* sequence. The sequence flanked by the *loxP* sites was recodonized to prevent homologous recombination during gene editing. Names and binding sites of the primers used for diagnostic PCRs are

915 indicated. **(B)** Diagnostic PCRs on gDNA of NF54/iKO-FKBP35 parasites confirm correct
916 locus editing and rapamycin-induced *loxP* recombination. Numbers at the bottom indicate the
917 expected band sizes. **(C)** DNA content analysis of FKBP35$^{\mathbf{KO}}$ and FKBP35$^{\mathbf{WT}}$ parasites in
918 presence or absence of isopentenyl pyrophosphate (IPP)-supplementation. Disruption of
919 isoprenoid precursor biosynthesis in the apicoplast – the only essential function of this organelle
920 – is a known cause for delayed death in *P. falciparum* (35, 36). Inhibition of isoprenoid
921 synthesis by doxycycline can thus be restored by supplementing the parasite culture medium
922 with the isoprenoid precursor IPP (79). However, IPP supplementation did not alter the fate of
923 FKBP35$^{\mathbf{KO}}$ cells, demonstrating that their death in G2 is independent of apicoplast-dependent
924 processes as shown by DNA content analysis. Doxycycline-treated wild-type parasites rescued
925 by IPP-supplementation served as positive control**.** The knockout was induced at 0-6 hpi.
926 Representative data of three biological replicates are shown. **(D)** Parasite survival after
927 exposure to 40 °C for 6 h. Given the reported interactions of *Pf*FKBP35 with heat shock protein
928 70 (HSP70) and HSP90 (14, 16), we tested the parasite`s response to heat stress. *Pf*HSP70 is
929 required to ensure parasite survival under heat shock conditions by stabilizing the digestive
930 vacuole membrane trough binding to phosphatidylinositol 3-phosphate (80). Despite this
931 association, we did not detect altered heat-susceptibility between FKBP35$^{\mathbf{KO}}$ and FKBP35$^{\mathbf{WT}}$
932 cells. The knockout was induced at 0-6 hpi. n=3, error bars represent the standard error of the
933 mean**. (E)** Assessment of translation rates using SUnSET. FKBP35^{KO} and FKBP35^{WT}
934 trophozoites of G1 were incubated with puromycin for 1 hour. Incorporated puromycin was
935 detected using an α-puromycin antibody; α-GAPDH served as loading control. Replicate 3 is
936 also shown in main figure 3 (mirrored). The control was performed using an NF54/DiCre
937 parasite line. Untreated control parasites were cultured in absence of puromycin, confirming
938 the specificity of the α-puromycin antibody.

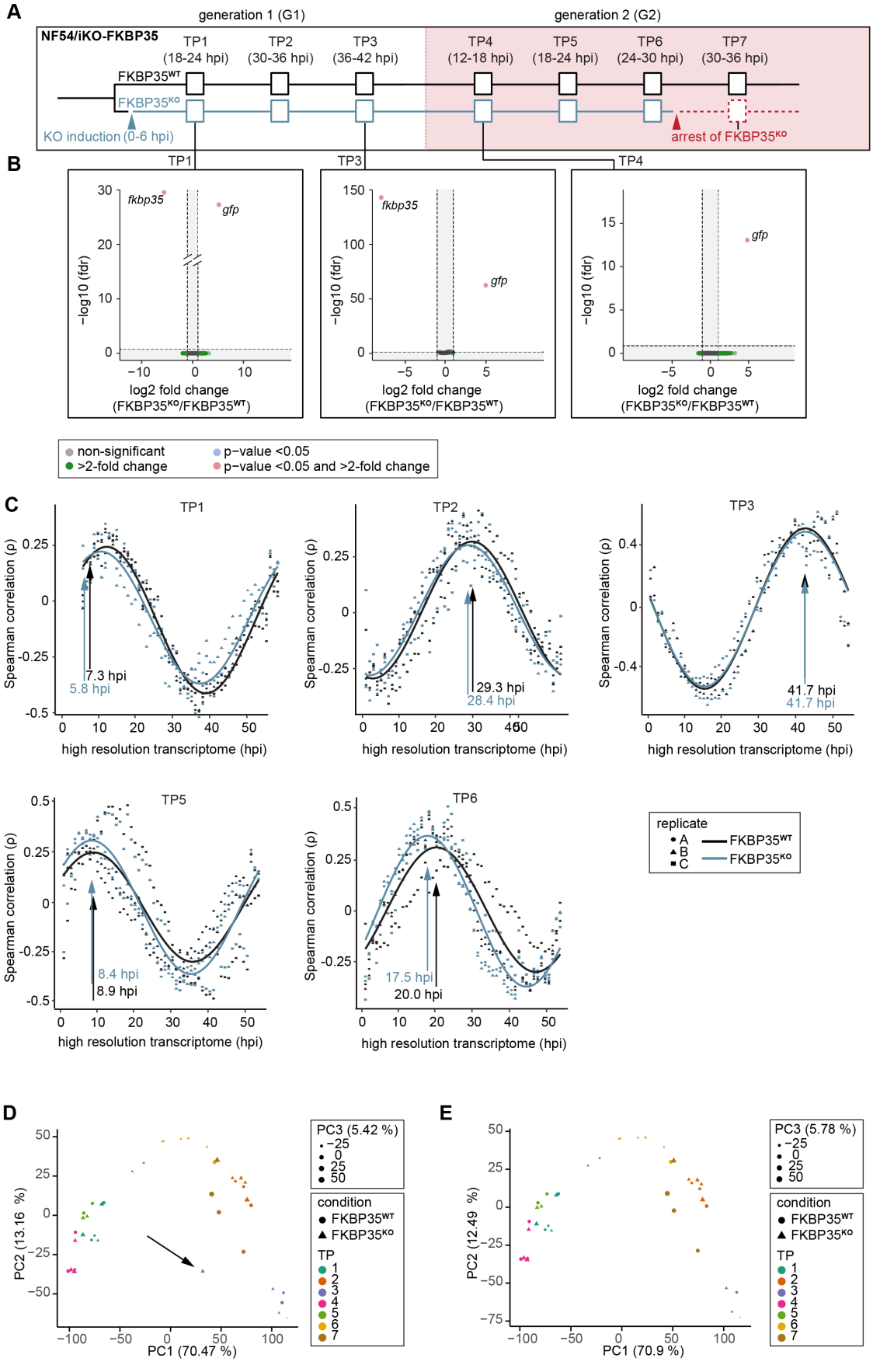

Figure S3. Transcriptomics reveals a cell cycle arrest of FKBP35^{KO} parasites.

941 **(A)** Schematic of the experimental setup. The knockout was induced at 0-6 hpi. RNA was
942 collected at indicated time points (TPs). **(B)** Volcano plots show differential gene expression
943 between $FKBP35^{KO}$ and $FKBP35^{WT}$ parasites. Genes are color-coded according to the fold
944 change and fdr (false discovery rate), n=3. **(C)** Mapping of $FKBP35^{\mathbf{KO}}$ and $FKBP35^{\mathbf{WT}}$
945 transcriptomes to a high-resolution reference data set (41). Spearman rank coefficients (ρ)
946 describe the correlation between the sampled transcriptomes and the reference data set. The
947 time points with the highest correlation coefficient are indicated. **(D)** Principal component
948 analysis (PCA) of RNA-Seq data by condition and time point (TP). The outlier at TP3
949 (highlighted by an arrow) was removed from the analysis. **(E)** PCA of RNA-Seq data by
950 condition and time point without the TP3 outlier mentioned in (D). Exclusion of this sample
951 did not affect the overall pattern.

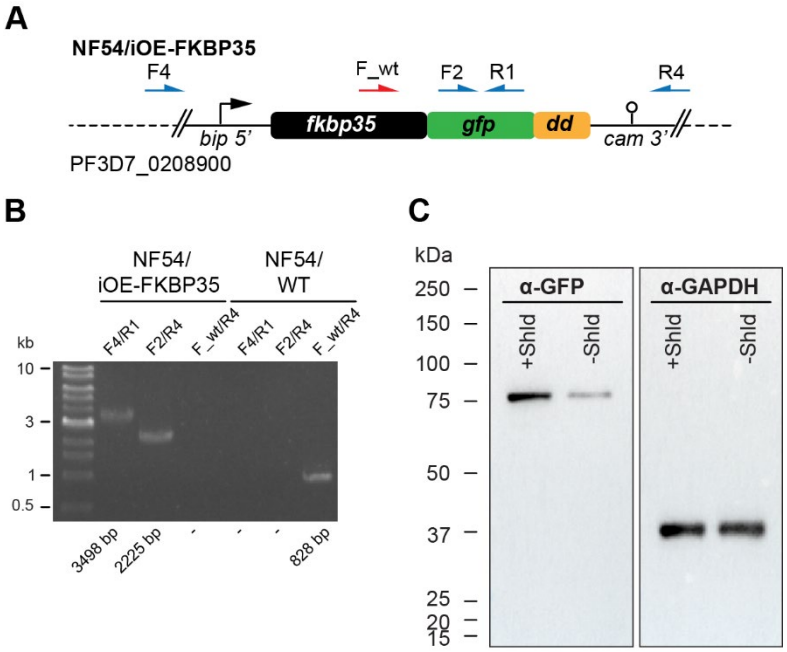

Figure S4. Characterization of NF54/iOE-FKBP35 parasites.

(A) Schematic of the modified *p230p* locus (PF3D7_0208900) in NF54/iOE-FKBP35 parasites, in which the overexpression cassette was introduced. This cassette consists of a *bip* promoter upstream of coding sequences of *fkbp35*, green fluorescent protein (*gfp*) and destabilization domain (*dd*), followed by the *cam 3'* region. Names and binding sites of the primers used for diagnostic PCRs are indicated. The primer F_wt only binds the unmodified *p230p* sequence. **(B)** Diagnostic PCRs performed on gDNA of NF54/iOE-FKBP35 parasites to confirm correct editing of the locus. PCRs performed on NF54/WT gDNA served as control. Numbers at the bottom indicate the expected band sizes. **(C)** Expression levels of the FKBP35-GFP-DD fusion protein were assessed by Western blot. Parasite cultures were split at 0-6 hpi and treated with Shield or the vehicle control EtOH. Protein lysates were collected 40 h later. α-GAPDH served as loading control. The expected size of the FKBP35-GFP-DD fusion protein is 74.2 kDa.

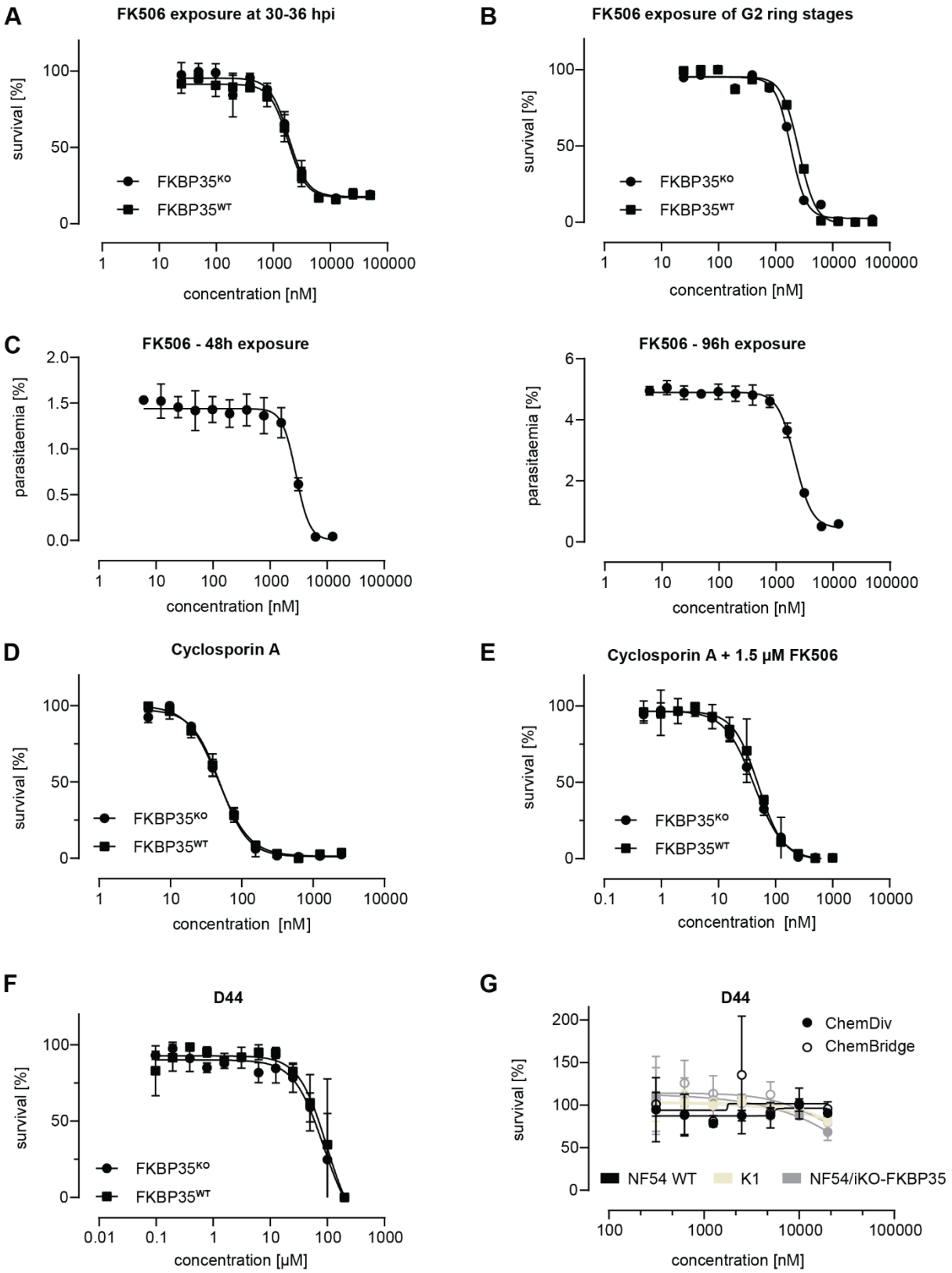

Figure S5. FKBP-targeting drugs fail at inhibiting parasite *Pf*FKBP35.

(A) Dose-response effect of FK506 on FKBP35^{KO} and FKBP35^{WT} parasites. The knockout was induced at 0-6 hpi and parasites were exposed to FK506 at 30-36 hpi. Survival rates were measured by flow cytometry in G2. n=3, error bars represent the standard error of the mean.

970 **(B)** Dose-response effect of FK506 on FKBP35^{KO} and FKBP35^{WT} parasites. The knockout was
971 induced at 34-40 hpi in G1. Ring stage parasites of G2 were exposed to FK506 for 48 hours
972 and survival rates were measured by flow cytometry in G3. Data points represent survival rates
973 measured in a single experiment performed in technical duplicates. **(C)** Dose-response effect of
974 FK506 on FKBP35^{WT} parasites over two IDCs. Parasites at 0-6 hpi were exposed to FK506 and
975 incubated for 96 hours. Parasitaemia was measured by flow cytometry after 48 hours and 96
976 hours. Medium containing the appropriate drug concentrations was changed after 48 hours. n=3,
977 error bars represent the standard error of the mean. **(D)** Dose-response effect of cyclosporin A
978 on FKBP35^{KO} and FKBP35^{WT} parasites. Cylocsporin A, a known inhibitor of calcineurin when
979 complexed with FKBP in other organisms (81), did not alter drug susceptibility between
980 FKBP35^{KO} and FKBP35^{WT} parasites, suggesting that *Pf*FKBP35 is not involved in regulating
981 calcineurin activity. The knockout was induced at 0-6 hpi. Parasites were exposed to
982 cyclosporin A for 48 hours. n=3, error bars represent the standard error of the mean. **(E)** Dose-
983 response effect of cyclosporin A in combination with a constant FK506 concentration on
984 FKBP35^{KO} and FKBP35^{WT} parasites. The knockout was induced at 0-6 hpi. Parasites were
985 subsequently exposed to cyclosporin A and 1.5 µM FK506 for 48 h. n=3, error bars represent
986 the standard error of the mean. **(F)** Dose-response effect of D44 on FKBP35^{KO} and FKBP35^{WT}.
987 The knockout was induced at 0-6 hpi and parasites were exposed to D44 for 48 hours thereafter.
988 Survival rates were determined using flow cytometry. n=3, error bars represent the standard
989 error of the mean. **(G)** Dose-response effect of D44 on NF54 WT, K1 and NF54/iKO-FKBP35
990 parasites after 72 h exposure. Survival rates were determined using a hypoxanthine
991 incorporation assay. Data points represent the mean of two technical replicates. Error bars
992 represent the standard error of the mean.

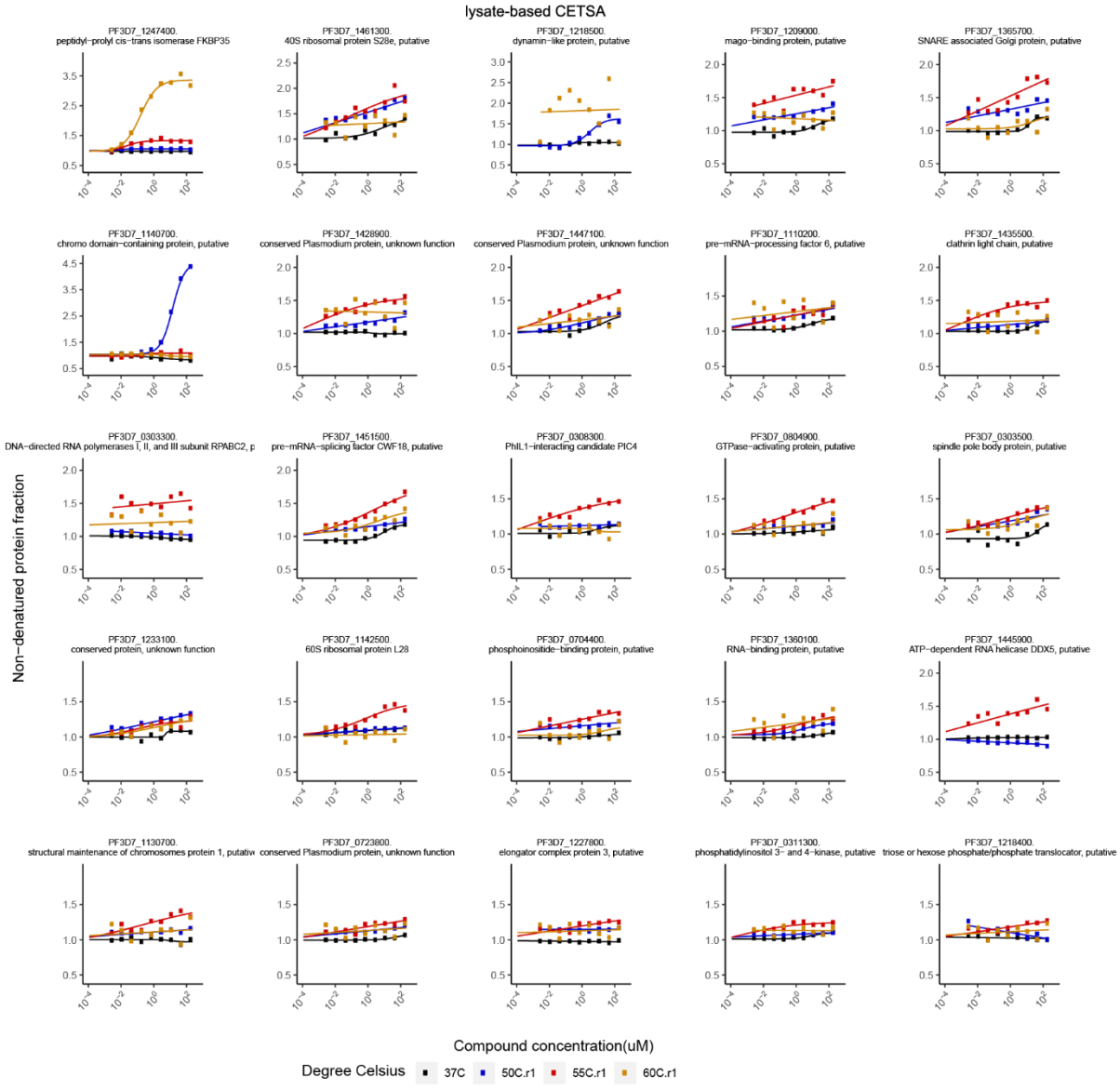

Figure S6. Putative FK506 interaction partners identified by protein lysate-based CETSA.

Proteins with an area under the curve (ΔAUC in protein lysate-based CETSA) greater than two median absolute deviations and an R^2 greater than 0.8 are listed. Bullets represent the abundance of non-denatured proteins in response to increasing FK506 concentrations under thermal challenge relative to a DMSO control. Colors indicate the temperatures used for protein denaturation; the black curve represents the non-denaturing control.

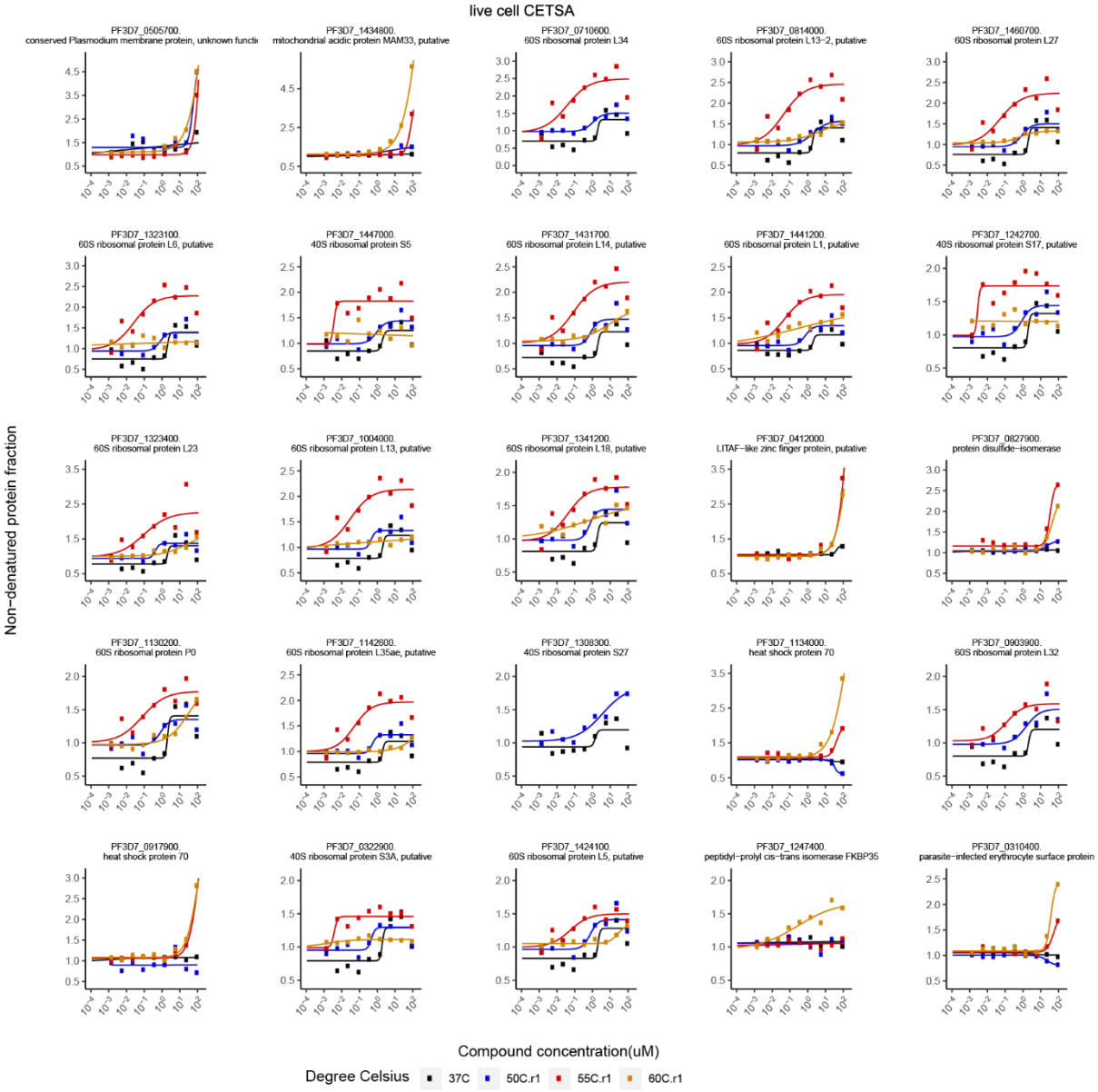

Figure S7. Putative FK506 interaction partners identified by live cell CETSA.

Proteins with an area under the curve (ΔAUC in live cell CETSA) greater than two median absolute deviations and an R^2 greater than 0.8 are listed. Bullets represent the abundance of non-denatured proteins in response to increasing FK506 concentrations under thermal challenge relative to a DMSO control. Colors indicate the temperatures used for heat challenge; the black curve represents the non-denaturing control.

1008 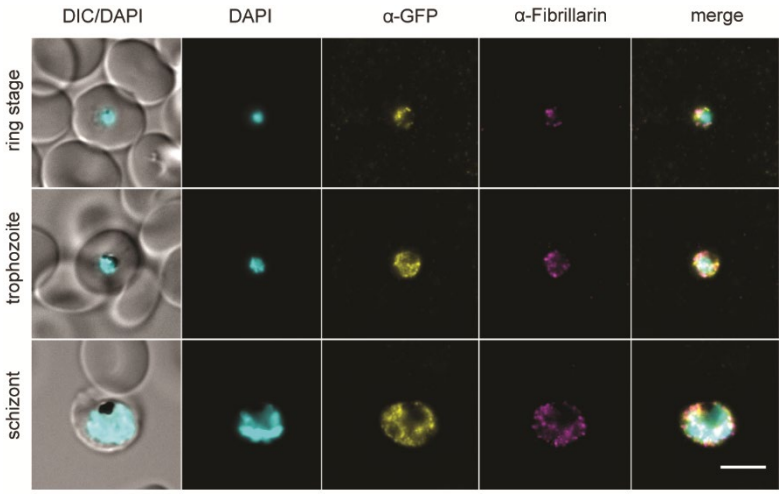

1009 **Figure S8. *Pf*FKBP35 localizes near fibrillarin-dense nuclear regions.**

1010 Localization of *Pf*FKBP35 (GFP) and fibrillarin in NF54/iKD-FKBP35 parasites at the ring,
1011 trophozoite and schizont stage assessed by immunofluorescence. DNA was stained with DAPI.
1012 Representative images are shown. Scale bar: 5 µm. DIC, differential interference contrast.

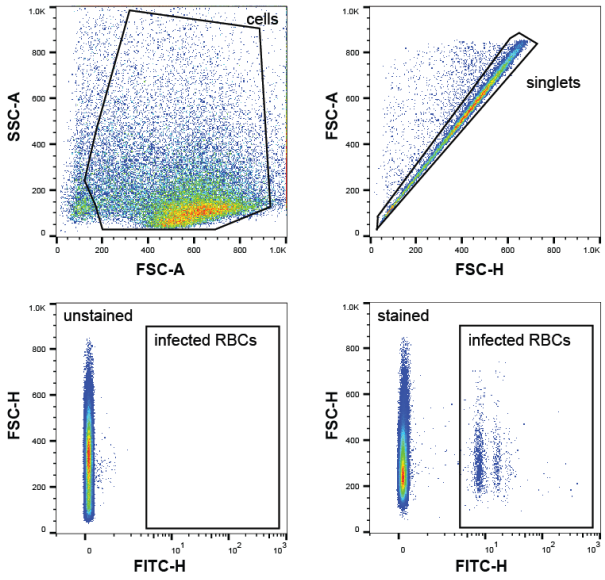

Figure S9. Gating strategy of flow cytometry data.

Representative flow cytometry plots of formaldehyde/glutaraldehyde-fixed parasite cultures are shown. The first plot shows the gate to distinguish cells from small debris (SSC-A vs. FSC-A). The 'singlets' gate (FSC-A vs. FSC-H) removes events with more than one cells. SYBR Green fluorescence intensity is used to identify parasite-infected RBCs (FSC-H vs. FITC-H). SSC, side scatter. FSC, forward scatter. FITC, fluorescein-5-isothiocyanate. A, area. H, height.

1020 **Table S1.** Mass spectrometry data comparing the proteomes of FKBP35^{KO} and FKBP35^{WT}
1021 parasites.

1022 **Table S2.** RNA-seq data comparing the transcriptomes of FKBP35^{KO} and FKBP35^{WT}
1023 parasites.

1024 **Table S3.** CETSA data showing the relative abundance of soluble proteins under non-
1025 denaturing and denaturing conditions in response to increasing FK506 concentrations.

1026 **Table S4.** Oligonucleotides used in this study.

1027

1028 # 5 References

1029 1. WHO. World malaria report 2022. Geneva: WHO; 2022.

1030 2. Ippolito MM, Moser KA, Kabuya JB, Cunningham C, Juliano JJ. Antimalarial Drug
1031 Resistance and Implications for the WHO Global Technical Strategy. Curr Epidemiol Rep.
1032 2021;8(2):46-62.

1033 3. Bell A, Wernli B, Franklin RM. Roles of peptidyl-prolyl cis-trans isomerase and
1034 calcineurin in the mechanisms of antimalarial action of cyclosporin A, FK506, and rapamycin.
1035 Biochem Pharmacol. 1994;48(3):495-503.

1036 4. Bharatham N, Chang MW, Yoon HS. Targeting FK506 binding proteins to fight
1037 malarial and bacterial infections: current advances and future perspectives. Curr Med Chem.
1038 2011;18(12):1874-89.

1039 5. Monaghan P, Bell A. A Plasmodium falciparum FK506-binding protein (FKBP) with
1040 peptidyl-prolyl cis-trans isomerase and chaperone activities. Mol Biochem Parasitol.
1041 2005;139(2):185-95.

1042 6. Bell A, Monaghan P, Page AP. Peptidyl-prolyl cis-trans isomerases (immunophilins)
1043 and their roles in parasite biochemistry, host-parasite interaction and antiparasitic drug
1044 action. Int J Parasitol. 2006;36(3):261-76.

1045 7. Kolos JM, Voll AM, Bauder M, Hausch F. FKBP Ligands-Where We Are and Where to
1046 Go? Front Pharmacol. 2018;9:1425.

1047 8. Kang CB, Hong Y, Dhe-Paganon S, Yoon HS. FKBP family proteins: immunophilins
1048 with versatile biological functions. Neurosignals. 2008;16(4):318-25.

1049 9. Bose S, Weikl T, Bügl H, Buchner J. Chaperone function of Hsp90-associated
1050 proteins. Science. 1996;274(5293):1715-7.

1051 10. Furutani M, Ideno A, Iida T, Maruyama T. FK506 binding protein from a thermophilic
1052 archaeon, methanococcus thermolithotrophicus, has chaperone-like activity in vitro.
1053 Biochemistry. 2000;39(10):2822.

1054 11. Yang WM, Yao YL, Seto E. The FK506-binding protein 25 functionally associates with
1055 histone deacetylases and with transcription factor YY1. Embo j. 2001;20(17):4814-25.

1056 12. Kasahara K, Nakayama R, Shiwa Y, Kanesaki Y, Ishige T, Yoshikawa H, et al. Fpr1,
1057 a primary target of rapamycin, functions as a transcription factor for ribosomal protein
1058 genes cooperatively with Hmo1 in Saccharomyces cerevisiae. PLoS Genet.
1059 2020;16(6):e1008865.

1060 13. Cardenas ME, Zhu D, Heitman J. Molecular mechanisms of immunosuppression by
1061 cyclosporine, FK506, and rapamycin. Curr Opin Nephrol Hypertens. 1995;4(6):472-7.

1062 14. Leneghan D, Bell A. Immunophilin-protein interactions in Plasmodium falciparum.
1063 Parasitology. 2015;142(11):1404-14.

1064 15. Yoon HR, Kang CB, Chia J, Tang K, Yoon HS. Expression, purification, and
1065 molecular characterization of Plasmodium falciparum FK506-binding protein 35 (PfFKBP35).
1066 Protein Expr Purif. 2007;53(1):179-85.

1067 16. Kumar R, Adams B, Musiyenko A, Shulyayeva O, Barik S. The FK506-binding protein
1068 of the malaria parasite, Plasmodium falciparum, is a FK506-sensitive chaperone with FK506-
1069 independent calcineurin-inhibitory activity. Mol Biochem Parasitol. 2005;141(2):163-73.

1070 17. Alag R, Bharatham N, Dong A, Hills T, Harikishore A, Widjaja AA, et al.
1071 Crystallographic structure of the tetratricopeptide repeat domain of Plasmodium falciparum
1072 FKBP35 and its molecular interaction with Hsp90 C-terminal pentapeptide. Protein Sci.
1073 2009;18(10):2115-24.

1074 18. Zhang M, Wang C, Otto TD, Oberstaller J, Liao X, Adapa SR, et al. Uncovering the
1075 essential genes of the human malaria parasite Plasmodium falciparum by saturation
1076 mutagenesis. Science. 2018;360(6388).

1077 19. Alag R, Qureshi IA, Bharatham N, Shin J, Lescar J, Yoon HS. NMR and
1078 crystallographic structures of the FK506 binding domain of human malarial parasite
1079 Plasmodium vivax FKBP35. Protein Sci. 2010;19(8):1577-86.

1080 20. Goh CKW, Silvester J, Wan Mahadi WNS, Chin LP, Ying LT, Leow TC, et al.
1081 Expression and characterization of functional domains of FK506-binding protein 35 from
1082 Plasmodium knowlesi. Protein Eng Des Sel. 2018;31(12):489-98.

1083 21. Bianchin A, Allemand F, Bell A, Chubb AJ, Guichou JF. Two crystal structures of the
1084 FK506-binding domain of Plasmodium falciparum FKBP35 in complex with rapamycin at high
1085 resolution. Acta Crystallogr D Biol Crystallogr. 2015;71(Pt 6):1319-27.

1086 22. Kotaka M, Ye H, Alag R, Hu G, Bozdech Z, Preiser PR, et al. Crystal structure of the
1087 FK506 binding domain of Plasmodium falciparum FKBP35 in complex with FK506.
1088 Biochemistry. 2008;47(22):5951-61.

1089 23. MacDonald CA, Boyd RJ. Computational insights into the suicide inhibition of
1090 Plasmodium falciparum Fk506-binding protein 35. Bioorg Med Chem Lett. 2015;25(16):3221-
1091 5.

1092 24. Harikishore A, Niang M, Rajan S, Preiser PR, Yoon HS. Small molecule Plasmodium
1093 FKBP35 inhibitor as a potential antimalaria agent. Sci Rep. 2013;3:2501.

1094 25. Harikishore A, Leow ML, Niang M, Rajan S, Pasunooti KK, Preiser PR, et al.
1095 Adamantyl derivative as a potent inhibitor of Plasmodium FK506 binding protein 35. ACS
1096 Med Chem Lett. 2013;4(11):1097-101.

1097 26. Rajan S, Yoon HS. Structural insights into Plasmodium PPIases. Front Cell Infect
1098 Microbiol. 2022;12:931635.

1099 27. MacDonald CA, Boyd RJ. Molecular docking study of macrocycles as Fk506-binding
1100 protein inhibitors. J Mol Graph Model. 2015;59:117-22.

1101 28. Deepa P, Thirumeignanam D. Understanding the potency of malarial ligand (D44) in
1102 plasmodium FKBP35 and modelled halogen atom (Br, Cl, F) functional groups. J Mol Graph
1103 Model. 2020;97:107553.

1104 29. Atack TC, Raymond DD, Blomquist CA, Pasaje CF, McCarren PR, Moroco J, et al.
1105 Targeted Covalent Inhibition of Plasmodium FK506 Binding Protein 35. ACS Med Chem Lett.
1106 2020;11(11):2131-8.

1107 30. Armstrong CM, Goldberg DE. An FKBP destabilization domain modulates protein
1108 levels in Plasmodium falciparum. Nat Methods. 2007;4(12):1007-9.

1109 31. Banaszynski LA, Chen LC, Maynard-Smith LA, Ooi AG, Wandless TJ. A rapid,
1110 reversible, and tunable method to regulate protein function in living cells using synthetic
1111 small molecules. Cell. 2006;126(5):995-1004.

1112 32. Collins CR, Das S, Wong EH, Andenmatten N, Stallmach R, Hackett F, et al. Robust
1113 inducible Cre recombinase activity in the human malaria parasite Plasmodium falciparum
1114 enables efficient gene deletion within a single asexual erythrocytic growth cycle. Mol
1115 Microbiol. 2013;88(4):687-701.

1116 33. Jones ML, Das S, Belda H, Collins CR, Blackman MJ, Treeck M. A versatile strategy
1117 for rapid conditional genome engineering using loxP sites in a small synthetic intron in
1118 Plasmodium falciparum. Sci Rep. 2016;6:21800.

1119 34. Kucharski M, Tripathi J, Nayak S, Zhu L, Wirjanata G, van der Pluijm RW, et al. A
1120 comprehensive RNA handling and transcriptomics guide for high-throughput processing of
1121 Plasmodium blood-stage samples. Malar J. 2020;19(1):363.

1122 35. Wiley JD, Merino EF, Krai PM, McLean KJ, Tripathi AK, Vega-Rodríguez J, et al.
1123 Isoprenoid precursor biosynthesis is the essential metabolic role of the apicoplast during
1124 gametocytogenesis in Plasmodium falciparum. Eukaryot Cell. 2015;14(2):128-39.

1125 36. Kennedy K, Cobbold SA, Hanssen E, Birnbaum J, Spillman NJ, McHugh E, et al.
1126 Delayed death in the malaria parasite Plasmodium falciparum is caused by disruption of
1127 prenylation-dependent intracellular trafficking. PLoS Biol. 2019;17(7):e3000376.

1128 37. Mi H, Ebert D, Muruganujan A, Mills C, Albou LP, Mushayamaha T, et al. PANTHER
1129 version 16: a revised family classification, tree-based classification tool, enhancer regions
1130 and extensive API. Nucleic Acids Res. 2021;49(D1):D394-d403.

1131 38. Boisvert FM, van Koningsbruggen S, Navascués J, Lamond AI. The multifunctional
1132 nucleolus. Nat Rev Mol Cell Biol. 2007;8(7):574-85.

1133 39. Plouffe D, Brinker A, McNamara C, Henson K, Kato N, Kuhen K, et al. In silico activity
1134 profiling reveals the mechanism of action of antimalarials discovered in a high-throughput
1135 screen. Proc Natl Acad Sci U S A. 2008;105(26):9059-64.

1136 40. Schmidt EK, Clavarino G, Ceppi M, Pierre P. SUnSET, a nonradioactive method to
1137 monitor protein synthesis. Nat Methods. 2009;6(4):275-7.

1138 41. Bozdech Z, Llinás M, Pulliam BL, Wong ED, Zhu J, DeRisi JL. The transcriptome of
1139 the intraerythrocytic developmental cycle of Plasmodium falciparum. PLoS Biol.
1140 2003;1(1):E5.

1141 42. Barnum KJ, O'Connell MJ. Cell cycle regulation by checkpoints. Methods Mol Biol.
1142 2014;1170:29-40.

1143 43. Monaghan P, Leneghan DB, Shaw W, Bell A. The antimalarial action of FK506 and
1144 rapamycin: evidence for a direct effect on FK506-binding protein PfFKBP35. Parasitology.
1145 2017;144(7):869-76.

1146 44. Van Duyne GD, Standaert RF, Karplus PA, Schreiber SL, Clardy J. Atomic structure
1147 of FKBP-FK506, an immunophilin-immunosuppressant complex. Science.
1148 1991;252(5007):839-42.

1149 45. Paul AS, Saha S, Engelberg K, Jiang RH, Coleman BI, Kosber AL, et al. Parasite
1150 Calcineurin Regulates Host Cell Recognition and Attachment by Apicomplexans. Cell Host
1151 Microbe. 2015;18(1):49-60.

1152 46. Desjardins RE, Canfield CJ, Haynes JD, Chulay JD. Quantitative assessment of
1153 antimalarial activity in vitro by a semiautomated microdilution technique. Antimicrob Agents
1154 Chemother. 1979;16(6):710-8.

1155 47. Dziekan JM, Yu H, Chen D, Dai L, Wirjanata G, Larsson A, et al. Identifying purine
1156 nucleoside phosphorylase as the target of quinine using cellular thermal shift assay. Sci
1157 Transl Med. 2019;11(473).

1158 48. Dziekan JM, Wirjanata G, Dai L, Go KD, Yu H, Lim YT, et al. Cellular thermal shift
1159 assay for the identification of drug-target interactions in the Plasmodium falciparum
1160 proteome. Nat Protoc. 2020;15(6):1881-921.

1161 49. Tan CSH, Go KD, Bisteau X, Dai L, Yong CH, Prabhu N, et al. Thermal proximity
1162 coaggregation for system-wide profiling of protein complex dynamics in cells. Science.
1163 2018;359(6380):1170-7.

1164 50. Ünal CM, Steinert M. FKBPs in bacterial infections. Biochim Biophys Acta.
1165 2015;1850(10):2096-102.

1166 51. Ng CL, Fidock DA. Plasmodium falciparum In Vitro Drug Resistance Selections and
1167 Gene Editing. Methods Mol Biol. 2019;2013:123-40.

1168 52. Kramer G, Patzelt H, Rauch T, Kurz TA, Vorderwülbecke S, Bukau B, et al. Trigger
1169 factor peptidyl-prolyl cis/trans isomerase activity is not essential for the folding of cytosolic
1170 proteins in Escherichia coli. J Biol Chem. 2004;279(14):14165-70.

1171 53. Gavigan CS, Kiely SP, Hirtzlin J, Bell A. Cyclosporin-binding proteins of Plasmodium
1172 falciparum. Int J Parasitol. 2003;33(9):987-96.

1173 54. Gudavicius G, Dilworth D, Serpa JJ, Sessler N, Petrotchenko EV, Borchers CH, et al.
1174 The prolyl isomerase, FKBP25, interacts with RNA-engaged nucleolin and the pre-60S
1175 ribosomal subunit. Rna. 2014;20(7):1014-22.

1176 55. Sydorskyy Y, Dilworth DJ, Halloran B, Yi EC, Makhnevych T, Wozniak RW, et al.
1177 Nop53p is a novel nucleolar 60S ribosomal subunit biogenesis protein. Biochem J.
1178 2005;388(Pt 3):819-26.

1179 56. Ferbitz L, Maier T, Patzelt H, Bukau B, Deuerling E, Ban N. Trigger factor in complex
1180 with the ribosome forms a molecular cradle for nascent proteins. Nature.
1181 2004;431(7008):590-6.

1182 57. Callebaut I, Mornon JP. Trigger factor, one of the Escherichia coli chaperone
1183 proteins, is an original member of the FKBP family. FEBS Lett. 1995;374(2):211-5.

1184 58. Rodriguez-Corona U, Sobol M, Rodriguez-Zapata LC, Hozak P, Castano E. Fibrillarin
1185 from Archaea to human. Biol Cell. 2015;107(6):159-74.

1186 59. Thiry M, Lafontaine DL. Birth of a nucleolus: the evolution of nucleolar compartments.
1187 Trends in cell biology. 2005;15(4):194-9.

1188 60. Lambros C, Vanderberg JP. Synchronization of Plasmodium falciparum erythrocytic
1189 stages in culture. J Parasitol. 1979;65(3):418-20.

1190 61. Trager W, Jenson JB. Cultivation of malarial parasites. Nature. 1978;273(5664):621-
1191 2.

1192 62. Brancucci NMB, Gerdt JP, Wang C, De Niz M, Philip N, Adapa SR, et al.
1193 Lysophosphatidylcholine Regulates Sexual Stage Differentiation in the Human Malaria
1194 Parasite Plasmodium falciparum. Cell. 2017;171(7):1532-44.e15.

1195 63. Filarsky M, Fraschka SA, Niederwieser I, Brancucci NMB, Carrington E, Carrió E, et
1196 al. GDV1 induces sexual commitment of malaria parasites by antagonizing HP1-dependent
1197 gene silencing. Science. 2018;359(6381):1259-63.

1198 64. Knuepfer E, Napiorkowska M, van Ooij C, Holder AA. Generating conditional gene
1199 knockouts in Plasmodium - a toolkit to produce stable DiCre recombinase-expressing
1200 parasite lines using CRISPR/Cas9. Sci Rep. 2017;7(1):3881.

1201 65. Gibson DG, Young L, Chuang RY, Venter JC, Hutchison CA, 3rd, Smith HO.
1202 Enzymatic assembly of DNA molecules up to several hundred kilobases. Nat Methods.
1203 2009;6(5):343-5.

1204 66. Ashdown GW, Dimon M, Fan M, Sánchez-Román Terán F, Witmer K, Gaboriau DCA,
1205 et al. A machine learning approach to define antimalarial drug action from heterogeneous
1206 cell-based screens. Sci Adv. 2020;6(39).

1207 67. Tibúrcio M, Yang ASP, Yahata K, Suárez-Cortés P, Belda H, Baumgarten S, et al. A
1208 Novel Tool for the Generation of Conditional Knockouts To Study Gene Function across the
1209 Plasmodium falciparum Life Cycle. mBio. 2019;10(5).

1210 68. Thommen BT, Passecker A, Buser T, Hitz E, Voss TS, Brancucci NMB. Revisiting the
1211 Effect of Pharmaceuticals on Transmission Stage Formation in the Malaria Parasite
1212 Plasmodium falciparum. Front Cell Infect Microbiol. 2022;12:802341.

1213 69. Thomas JA, Collins CR, Das S, Hackett F, Graindorge A, Bell D, et al. Development
1214 and Application of a Simple Plaque Assay for the Human Malaria Parasite Plasmodium
1215 falciparum. PLoS One. 2016;11(6):e0157873.

1216 70. Daubenberger CA, Tisdale EJ, Curcic M, Diaz D, Silvie O, Mazier D, et al. The N'-
1217 terminal domain of glyceraldehyde-3-phosphate dehydrogenase of the apicomplexan
1218 Plasmodium falciparum mediates GTPase Rab2-dependent recruitment to membranes. Biol
1219 Chem. 2003;384(8):1227-37.

1220 71. Ahrné E, Glatter T, Viganò C, Schubert C, Nigg EA, Schmidt A. Evaluation and
1221 Improvement of Quantification Accuracy in Isobaric Mass Tag-Based Protein Quantification
1222 Experiments. J Proteome Res. 2016;15(8):2537-47.

1223 72. Ritchie ME, Phipson B, Wu D, Hu Y, Law CW, Shi W, et al. limma powers differential
1224 expression analyses for RNA-sequencing and microarray studies. Nucleic Acids Res.
1225 2015;43(7):e47.

1226 73. McLean KJ, Jacobs-Lorena M. Plasmodium falciparum Maf1 Confers Survival upon
1227 Amino Acid Starvation. mBio. 2017;8(2).

1228 74. Kim D, Paggi JM, Park C, Bennett C, Salzberg SL. Graph-based genome alignment
1229 and genotyping with HISAT2 and HISAT-genotype. Nat Biotechnol. 2019;37(8):907-15.

1230 75. Aurrecoechea C, Brestelli J, Brunk BP, Dommer J, Fischer S, Gajria B, et al.
1231 PlasmoDB: a functional genomic database for malaria parasites. Nucleic Acids Res.
1232 2009;37(Database issue):D539-43.

1233 76. Love MI, Huber W, Anders S. Moderated estimation of fold change and dispersion for
1234 RNA-seq data with DESeq2. Genome Biol. 2014;15(12):550.

1235 77. Blighe K, Rana S, Lewis M. EnhancedVolcano: Publication-ready volcano plots with
1236 enhanced colouring and labeling. R package version 1.16.0.
1237 https://githubcom/kevinblighe/EnhancedVolcano. 2022.

1238 78. Kassambara A. ggcorrplot: Visualization of a Correlation Matrix using 'ggplot2'. R
1239 package version 0.1.3, . https://CRANR-projectorg/package=ggcorrplot. 2022.

1240 79. Yeh E, DeRisi JL. Chemical rescue of malaria parasites lacking an apicoplast defines
1241 organelle function in blood-stage Plasmodium falciparum. PLoS Biol. 2011;9(8):e1001138.

1242 80. Lu KY, Pasaje CFA, Srivastava T, Loiselle DR, Niles JC, Derbyshire E.
1243 Phosphatidylinositol 3-phosphate and Hsp70 protect Plasmodium falciparum from heat-
1244 induced cell death. Elife. 2020;9.

1245 81. Dumont FJ. FK506, an immunosuppressant targeting calcineurin function. Curr Med
1246 Chem. 2000;7(7):731-48.

1247